Psilocybin-enhanced fear extinction linked to bidirectional modulation of cortical ensembles

Sophie A. Rogers [1, 2], Elizabeth A. Heller [3], Gregory Corder [1, 2] ✉

[1] Department of Psychiatry, Perelman School of Medicine, University of Pennsylvania, Philadelphia, PA, 19104

[2] Department of Neuroscience, Mahoney Institute for Neurosciences, Perelman School of Medicine, University of Pennsylvania, Philadelphia, PA, 19104

[3] Department of Systems Pharmacology and Translational Therapeutics, Perelman School of Medicine, University of Pennsylvania, Philadelphia, PA, 19104

✉ Correspondence: gcorder@upenn.edu (G.C.)

Summary.

The serotonin 2 receptor (5HT2R) agonist psilocybin has demonstrated rapid and long-lasting efficacy across neuropsychiatric disorders characterized by cognitive inflexibility. Psilocybin may accomplish this by inducing rapid and stable dendritic plasticity. However, the impact of psilocybin on patterns of neural activity underlying sustained changes in cognitive and behavioral flexibility has not been characterized. To test the hypothesis that psilocybin enhances behavioral flexibility by rapidly and persistently altering activity in cortical neural ensembles, we performed longitudinal single-cell calcium imaging in the retrosplenial cortex across a five-day trace fear learning and extinction assay. Leveraging tensor component analysis to identify neurons that modulate activity on multiple temporal scales, we found that a single-dose of psilocybin induced cortical ensemble turnover between fear learning and extinction days while oppositely modulating activity in fear- and extinction- active neurons. The extent of suppression of fear-active neurons and recruitment of extinction-active neurons were both predictive of psilocybin-enhanced fear extinction. These results both align with hypotheses that psilocybin enhances behavioral flexibility by recruiting new populations of neurons and introduce a new mechanism involving the suppression of fear-active populations in the retrosplenial cortex.

Introduction.

Neuropsychiatric disorders characterized by inflexible associative learning, such as depression, anxiety, SUDs, and PTSD, affect over 350 million people worldwide[1]. Serotonergic psychedelics, including psilocybin, have demonstrated remarkable transdiagnostic potential across these disorders[2]. After only a single dose of psilocybin, many patients report long-lasting improvements in depression and SUDs, as well as overall well-being *for up to a year*—a timespan implicating the involvement of cortically mediated long-term memory[3–6]. Therapeutic-like effects also have been observed in rodent models in many behavioral studies[7–15], enabling the study of the neural mechanisms of psilocybin-enhanced mental health outcomes in mice.

Psilocybin is a naturally occurring compound found in hundreds of species of mushroom. Upon first pass metabolism, psilocybin is dephosphorylated into its active metabolite psilocin – a potent serotonin receptor agonist[16,17]. While psilocybin's subjective effects tend to be accompanied by feelings of extreme "bliss", "unity", and "meaningfulness"[2,18], in a subset of patients, psilocybin can induce extremely anxiogenic and even traumatic experiences, in some cases associated with long-term psychosis and suicidal ideation[19–22]. A variety of factors can contribute to whether a person will have a "good or bad trip," including genetic or endophenotypic predispositions[23,24], mindset or mood prior drug consumption (set), and environment in which the drug is consumed (setting)[25–30]. To develop safe therapies with minimal adverse side-effects, it is critical to identify the relevant neural subpopulations targeted by psilocybin and how they are differentially modulated to produce long-lasting therapeutic effects.

Clinical researchers have demonstrated that the therapeutic effects of serotonergic psychedelics in humans are mediated by increased cognitive flexibility following drug experience, a finding recapitulated in rodent models[31–34]. Cognitive *in*flexibility, or the inability to adapt thought or behavior to new environmental demands, is central to a wide range of neuropsychiatric disease[35,36]. Evidence from human, rodent, and molecular research converges on the hypothesis that psilocybin generates highly plastic brain states conducive to modifying circuits that underlie inflexible, maladaptive behaviors via 5HT2R and TrkB activation[2,17,37–44]. Acute activation of cortical neurons by psychedelics induces synaptic AMPA receptor insertion, BDNF signaling, and consequent dendritic growth[40,43,45,46]. It is unknown how these molecular actions of psilocybin impact information processing in those neural ensembles associated with aversive memories and maladaptive behavioral patterns.

The retrosplenial cortex (RSC) is one region where psilocybin may alter information processing in a manner sustaining enhanced cognitive flexibility. The RSC implements a variety of abstract functions[47], including encoding and retrieval of episodic memory[48–51]; imagination of the future[47]; value and context encoding [52–56]; egocentric navigation and reasoning[57–59]; and ego dissolution under psychedelics[60]. Chemogenetically inhibiting RSC during reversal learning impairs performance after a rule switch, suggesting RSC activity is crucial for cognitive flexibility[54]. In another study, Wang et al., 2019 identified a previously silent ensemble recruited in RSC during contextual fear extinction, another form of cognitive flexibility[61]. When the authors optogenetically reactivated this ensemble after re-conditioning, extinction was reinstated, suggesting that excitatory plasticity in the RSC drives fear extinction. The increase in c-FOS-expressing neurons after extinction observed by Wang et al. was recently replicated and shown to be sex-independent[62].

Several lines of evidence suggests that psilocybin's effects could in part be mediated by changes in RSC activity. Psilocybin increases c-FOS expression throughout the cortex but suppresses low- and enhances high-frequency neural oscillations specifically in the RSC[63,64]. While 5HT2ARs are distributed throughout cortical L5 pyramidal neurons, the RSC is the only cortical region that also contains 5HT2CRs on pyramidal neurons as opposed to GABAergic interneurons[65,66]. In humans with depression, functional connectivity between the serotonergic dorsal raphe nuclei and posterior cingulate regions homologous to rodent RSC is impaired[67]. Subsequent improvements in functional connectivity between the posterior cingulate and prefrontal cortex predict psilocybin-induced enhancements in cognitive flexibility[20]. Importantly, the RSC is involved in the retrieval of remote fear memories, positioning it as a potential substrate for psilocybin's longer-lasting effects[68–72].

To investigate the role of the RSC in the post-acute effects of psilocin on cognitive flexibility, extinction of trace fear conditioning (TFC) was employed as the appropriate primary behavioral paradigm. TFC is a model of complex fear learning in rodents, in which a conditioned stimulus (CS) is followed by a trace period of 20 sec preceding the shock. Importantly, the trace period in TFC distinguishes amygdala-dependent FC from cortex-dependent FC as it requires protracted attention to form an association between two temporally distant stimuli [73–75]. During extinction, the shock is omitted, and the animals must update their CS association to learn that it is now safe to reduce their freezing response, or extinguish. In mice, Kwapis et al. found that TFC extinction depends on excitatory activity in the RSC[73]. Others have shown that optical, electrolytic, and pharmacological interventions in the RSC impact various kinds and stages of FC[51,55,56,61,68-72,74-76]. In a one-day paradigm, psilocybin administered 24 hours prior facilitated TFC extinction before training at low doses[77]. However, this study did not investigate the effect of psilocybin on long-term, consolidated fear memory, which is of translational interest.

To test the hypothesis that psilocybin promotes cognitive flexibility by rapidly and persistently altering RSC ensembles associated with aversive memories, we investigated the effects of a single dose of psilocybin in a multi-day TFC extinction paradigm[77]. We then repeated this experiment in GCaMP8m-expressing, miniature microendoscope-implanted mice to measure single-cell calcium activity throughout the task. Using tensor component analysis (TCA)[78], we were able to identify ensembles driving RSC activity during different cognitive phases of the task - acquisition, early extinction/fear recall, and late extinction. We

were able to confirm our hypothesis that psilocybin accelerates and enhances the recruitment of an extinction-associated ensemble, particularly in drug-responsive animals. To our surprise, we found that psilocybin-enhanced fear extinction was also associated with an acute, robust suppression of fear-associated neurons. Taken together, these results support two mechanisms of psilocybin-enhanced fear extinction in the RSC, based on opposing forms of plasticity, which must act in concert to reduce cognitive inflexibility.

Results.

Psilocybin enhances TFC extinction in a responsive subpopulation of mice.

First, we aimed to expand on the results in Catlow et al. 2013, where the authors showed that mice injected with 1.0 mg/kg of psilocybin 24 hours before training both acquired and extinguished TFC more rapidly and completely than saline-administered mice[76]. Here, mice underwent a five-day TFC paradigm (**Fig. 1A**). On Day 1, mice underwent *Habituation*, during which mice were placed in a chamber with a smooth white floor insert and cleaned with ethanol (Context A). Mice listened to the CS play eight times. The CS consisted of a 4 kHz tone at 75 dB, delivered in one 200 ms pip/sec for 25 sec. During *Acquisition* on Day 2, the floor insert was removed, revealing the metal grid, and the boxes were cleaned with Clidox (Context B). Each of eight CS presentations was followed by a 20 sec trace period, after which a 1 mA, 2 sec shock was delivered. Each trial on every day consisted of the 25 sec CS, the 20 sec trace period, and the 2 sec shock or omission period. The inter-trial interval each trial was jittered 60±10 sec. During Days 3-5, mice un-

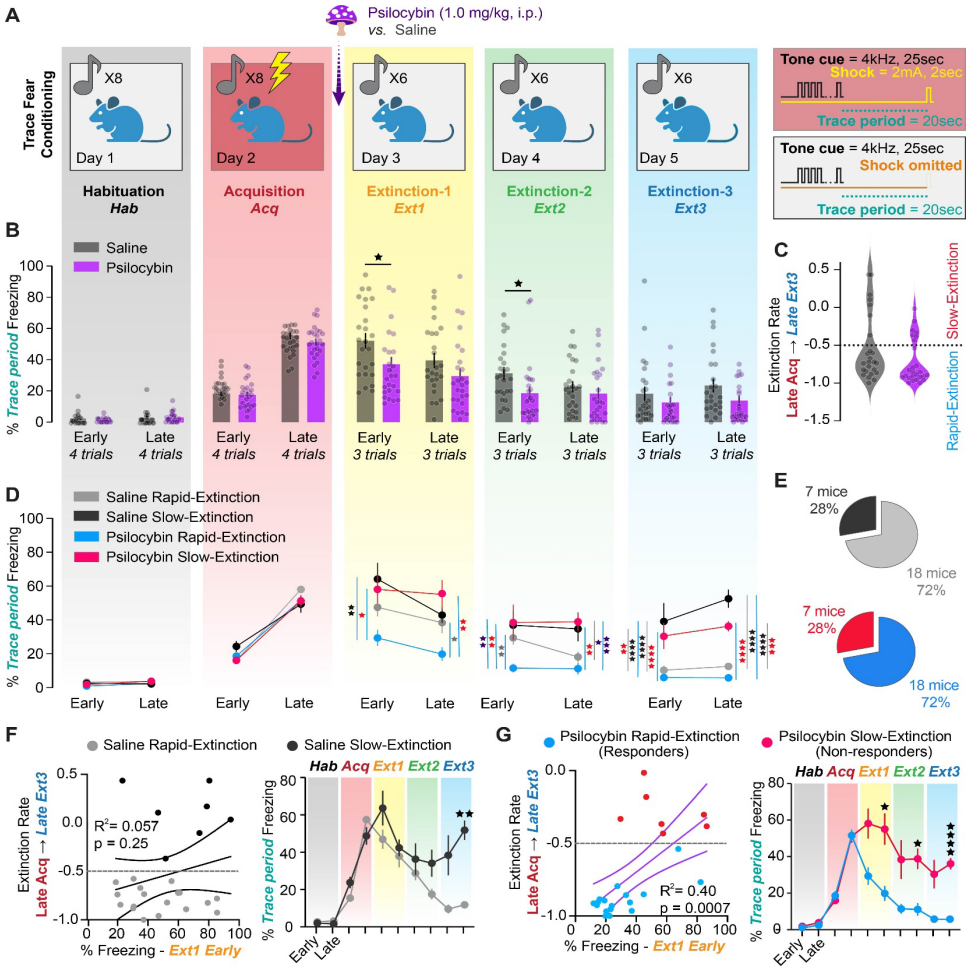

Figure 1 | Psilocybin enhances TFC extinction in a responsive subpopulation of mice.
(A) Diagram of five-day TFC experiment. Right-hand panels depict conditioned and unconditioned one parameters. **(B)** Average % time freezing during trace period in the first and last 3 trials of each day ("Early," "Late" respectively) in saline and psilocybin-administered mice (black and purple respectively, n=25 each). Dots are individual animals. Two-Way ANOVA with Sidak multiple comparisons correction (Supp. Table 1, rows 1-5). **(C)** Extinction rate calculated as the difference between freezing during late Acquisition and late Extinction 3 divided by freezing during late Acquisition. Red line indicates -50% threshold distinguishing rapidly- from slowly-extinguishing mice. Unpaired t-test. (Supp. Table 1, rows 6). **(D)** Same as B; treatment groups subdivided into rapid- and slow-extinguishing mice (light colors, rapid; dark colors, slow). Two-Way ANOVA with Sidak multiple comparisons correction. (Supp. Table 1, rows 7-11). **(E)** Pie charts describing breakdown of rapid- and slow-extinguishing mice within treatment groups. **(F)** *Left*: Linear regression predicting extinction rate based on % time freezing during early *Extinction 1* during acute drug treatment in saline-administered mice. *Right*: Direct comparison of % freezing over time between saline rapid- and slow-extinguishing mice. Two-Way ANOVA.(Supp. Table 1, rows 12-13). **(G)** Same as F for psilocybin-administered mice. (Supp. Table 1, rows 14-15).
Data are represented as mean ± SEM. * p ≤ 0.05, ** p < 0.01, *** p < 0.001, **** p < 0.0001

derwent *Extinction* sessions (*Extinction 1-3*), which consisted of 6 trials each in Context A with no shock. Freezing was measured in ezTrack[79] as percent of time immobile during the trace period.

Mice were administered psilocybin (1.0 mg/kg, i.p.) or saline 30 min before *Extinction 1*. This time-point was chosen as psilocybin-induced head twitches, the behavior taken as a proxy for the subjective effects in animals, peak around 15 min and last for up to 150 min[42]. Psilocybin acutely reduced freezing during the first (early) and last (late) three trials of *Extinction 1* compared to saline (**Fig. 1B**). Psilocybin also reduced freezing in early *Extinction 2*, and by *Extinction 3* there was no difference between groups (**Fig. 1B, Supp. Fig. 1A, Supp. Table 1**). Overall, there was no difference between males and females in either condition (**Supp. Fig. 1B & C, Supp. Table 1).**

The extinction rate was calculated as the percent difference between freezing in late *Acquisition* and late *Extinction 3*. Notably, there was a trend towards psilocybin-enhanced extinction rate, with a bimodal distribution of extinction rates of psilocybin and saline (**Fig. 1C, Supp. Table 1**). This bimodal distribution of percent freezing behavior was a stable feature of both the psilocybin and saline groups across the extinction sessions (**Fig. 1B,C**). As extinction rate was one of our primary outcomes, mice that had extinguished >50% of their late *Acquisition* freezing by late *Extinction 3* were classified as rapidly extinguishing and all others as slowly extinguishing.

Intriguingly, psilocybin-administered, rapidly extinguishing mice reduced freezing more strongly and quickly than all other groups (**Fig. 1D, Supp. Table 1**). These mice began freezing significantly less than saline-administered rapidly extinguishing mice during *Extinction 1*, suggesting psilocybin acutely blocks expression of fear memory recall. However, this effect persisted for the subsequent two days, suggesting that the extinction memory formed during *Extinction 1* persists and continues to be reinforced more strongly in psilocybin rapidly extinguishing mice than saline rapidly extinguishing mice during *Extinction 2*. In contrast, freezing in slowly extinguishing mice was unaffected by treatment (**Fig. 1D, Supp. Table 1).** There was the same proportion of rapid and slow extinguishing mice in each group (**Fig. 1E**).

Because slow extinguishing mice were indistinguishable based on psilocybin or saline treatments, we wondered whether there was subpopulation of psilocybin non-responsive mice or whether it is always the case that mice that freeze more during recall extinguish slowly. To address this question, linear regression was performed to determine whether percent freezing during the psilocybin's acute effects in early *Extinction 1* would predict extinction rate. Compellingly, a linear model fit psilocybin but not saline, while clustering rapid- and slow-extinguishers together (**Fig. 1F & G, Supp. Table 1).** Logistic regression was therefore also used to classify mice as rapid or slow based on their early *Extinction 1* freezing alone. (**Supp. Fig. 1E & F, Supp. Table 1**) Based on area under the receiver operator characteristic curve analysis, the percent freezing during *Extinction 1* predicted classification as either rapidly or slowly extinguishing only if mice were administered psilocybin (auROC = 0.8333, p = 0.0077), but not saline (auROC = 0.6032, p = 0.4314). Thus, we identified a classes of psilocybin-responsive and non-responsive mice, hereon referred to as "*responders*" and "*non-responders*" respectively.

Miniscope-implanted mice acquire and extinguish TFC.

To explore the neurophysiological correlates of psilocybin-enhanced TFC extinction, single cell calcium activity was recorded in the retrosplenial cortex (RSC) of saline and psilocybin mice. Mice were injected with AAV9-*hSyn*-GCaMP8m in the RSC (right hemisphere) and two weeks later implanted with a 1.0 mm diameter, gradient refractive index lens (GRIN) over the injection site (**Fig. 2A, B**). After 2-5 weeks, mice were trained in the same TFC task (**Fig. 2C**). Calcium traces were extracted using CNMF-E in the Inscopix Data Processing Software API and post-processed (**Fig. 2D**). Across the entire TFC imaging protocol, 11-160 RSC neurons per animal (median = 46) were longitudinally registered across all days (Psilocybin responders = 460 total neurons; Psilocybin non-responders = 350 total neurons; Saline = 357 total neurons; **Fig. 2E,G,H**). Miniscope placements were validated in all mice (**Supp. Fig. 2**).

All of the n=21 Miniscope mice successfully acquired fear learning (average >20% freezing throughout *Acquisition*, and >10% during early *Extinction 1*), and were subsequently split into psilocybin (1.0 mg/kg; i.p.; n=14 mice) and saline (n=7 mice; **Fig. 2F left**). Unlike the psilocybin mice in Figure 1, no acute effect of psilocybin was observed on fear recall (**Fig. 2F right, Supp. Table 1**). Nonetheless, by *Extinction 3,* a subset of psilocybin responders emerged. Seven psilocybin mice extinguished their freezing by over 50% (**Fig. 2F, Supp. Table 1**), freezing significantly less than saline controls and non-responders during *Extinction 3* (**Fig. 2F, Supp. Table 1**). Though behavior in Miniscope-implanted mice displayed great variance, the distributions of extinction rate in each group appear consistent with those in non-implanted animals (**Fig. 2F right, Fig. 1C**).

RSC neurons are modulated over TFC training.

To determine changes in the task-relevant response properties of RSC neurons, fractions of tone-, trace, shock-, and tone+trace-responsive neurons were measured each day (**Fig. 2I**). Fractions of tone- or trace period-upregulated neurons were not significantly affected over time in any treatment group and in general varied between 10-30% of neurons (**Fig. 2J & K, Supp. Table 1**). Approximately ~40% of recorded RSC neurons were shock-responsive neurons (**Fig. 2L, Supp. Table 1**). On average, ~50% of tone-responsive neurons on a given day were also trace-responsive on the same day, suggesting a high degree of overlap of activated neurons between different periods in a trial (**Fig. 2M, Supp. Table 1**). There was a large rate of turnover in tone- and trace-responsive neurons between days, with ~75% of tone- and ~60% trace-responsive neurons maintaining their

responsiveness for only 1 day and about ~25% and ~30% respectively for 2 days across groups (**Fig. 2N & O**).

Finally, the RSC was host to many neurons encoding freezing behavior in every session (**Supp. Fig. 2B**). Interestingly, the average freezing encoding of individual neurons increased during *Acquisition*, suggesting that RSC neurons preferentially encode acute fear-related freezing (**Fig. 2P & Q, Supp. Table 1**). None of these observations were affected by treatment.

Tensor component analysis (TCA) reveals evolution of RSC through different states over fear and extinction learning.

We hypothesized that psilocybin induces the rapid recruitment of a novel *Extinction* associated ensemble in the

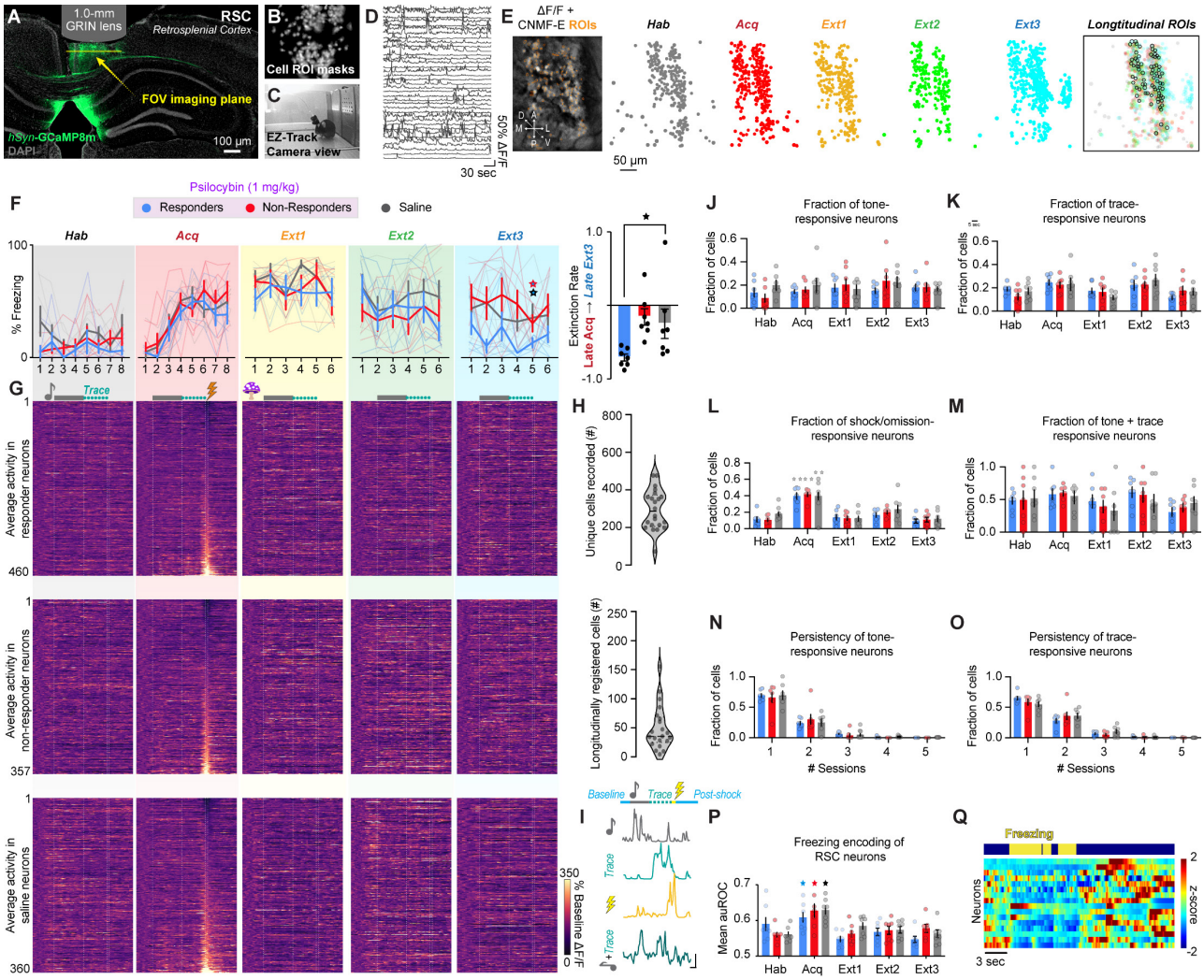

Figure 2 | RSC neurons are modulated over TFC extinction in psilocybin- and saline-administered mice.
(A) Representative image of *AAV8-syn-GCaMP8m-WPRE* expression (green) and nuclei (grey) in RSC under GRIN lens tract. **(B)** Cell masks of imaged neurons during one session from same mouse. **(C)** Image of behavioral set-up during an extinction session. Example frame of freezing mouse. **(D)** Example traces of neurons recorded during behavior in dF/F in same mouse. **(E)** Left: Representative image from Ca^{2+}-imaging video in the same mouse. Right: Cell masks of each recorded neuron in each session, overlayed with masks of longitudinally registered cells. **(F)** *Left*: Percent of time freezing during each trial in responders (n=7 mice), non-responders (n=7 mice), and saline mice (n=7 mice). Two-Way ANOVA. (Supp. Table 1, rows 16-20) *Right*: Extinction rate. One-Way ANOVA with Tukey multiple comparisons corrections. (Supp. Table 1, row 21). **(G)** Average activity in each neuron over all trials from each session, normalized to baseline before one onset and aligned to shock. Top: Responders (n=460 neurons), Middle: Non-responders (n=350 neurons), Bottom: Saline (n=360 neurons). **(H)** *Top*: Number of unique cells accepted over all sessions in each animals. *Bottom*: Number of longitudinally registered neurons in each animal. **(I)** Example traces of tone-, trace-, shock, and tone+trace-responsive neurons (top to bottom). Vertical scale bar = 2dF/F, horizontal scale bar = 5 sec. **(J)** Fraction of tone-responsive cells in each group over each day. Two-Way ANOVA. (Supp. Table 1, row 22). **(K)** Fraction of trace-responsive cells in each group over each day. Two-Way ANOVA. (Supp. Table 1, row 23). **(L)** Fraction of shock/omission-responsive cells in each group over each day. Two-Way ANOVA. (Supp. Table 1, row 24). **(M)** Fraction of one-responsive neurons that are also trace-responsive cells in each group over each day. Two-Way ANOVA. (Supp. Table 1, row 25). **(N)** Fraction of one-responsive cells that are one-responsive for 1-5 days in each animal. **(O)** Fraction of trace-responsive cells that are trace-responsive for 1-5 days in each animal. **(P)** Average freezing encoding of neurons in each group over each day (auROC, Two-Way ANOVA). (Supp. Table 1, row 26). **(Q)** Representative traces of freezing-encoding neurons in 1 animal sorted from greatest to least (bottom to top) auROC.
Data are represented as mean ± SEM. * $p \leq 0.05$, ** $p < 0.01$, *** $p < 0.001$, **** $p < 0.0001$

RSC during *Extinction 1* that persistently drives RSC activity during future extinction sessions. Additionally, enhanced extinction could arise from psilocybin-mediated suppression of specific ensembles associated with the fear learning and memory. Therefore, to identify ensembles associated with TFC acquisition and extinction, we employed a technique developed by Williams et al., 2018 called Tensor Component Analysis (TCA)[78]. (**Fig. 3A**) TCA, like PCA or principal component analysis, is an unsupervised dimensionality reduction technique that can be used to group neurons into functional ensembles defined by their within- and across-trial dynamics. Unlike PCA, TCA has no orthogonality constraint or unique solution. The lack of orthogonality constraint bestows the immense benefit of interpretability – in the present task, for instance, "fear recall" trials are not orthogonal to "fear extinction" trials. To validate models constructed via TCA, it is necessary to run multiple iterations of the algorithm, comparing the models' reconstruction error and similarity to ensure the model used for subsequent analysis is not caught in a rare, non-optimal local minimum.

To determine the appropriate model rank for analysis, TCA was run on cells pooled from all animals in a given

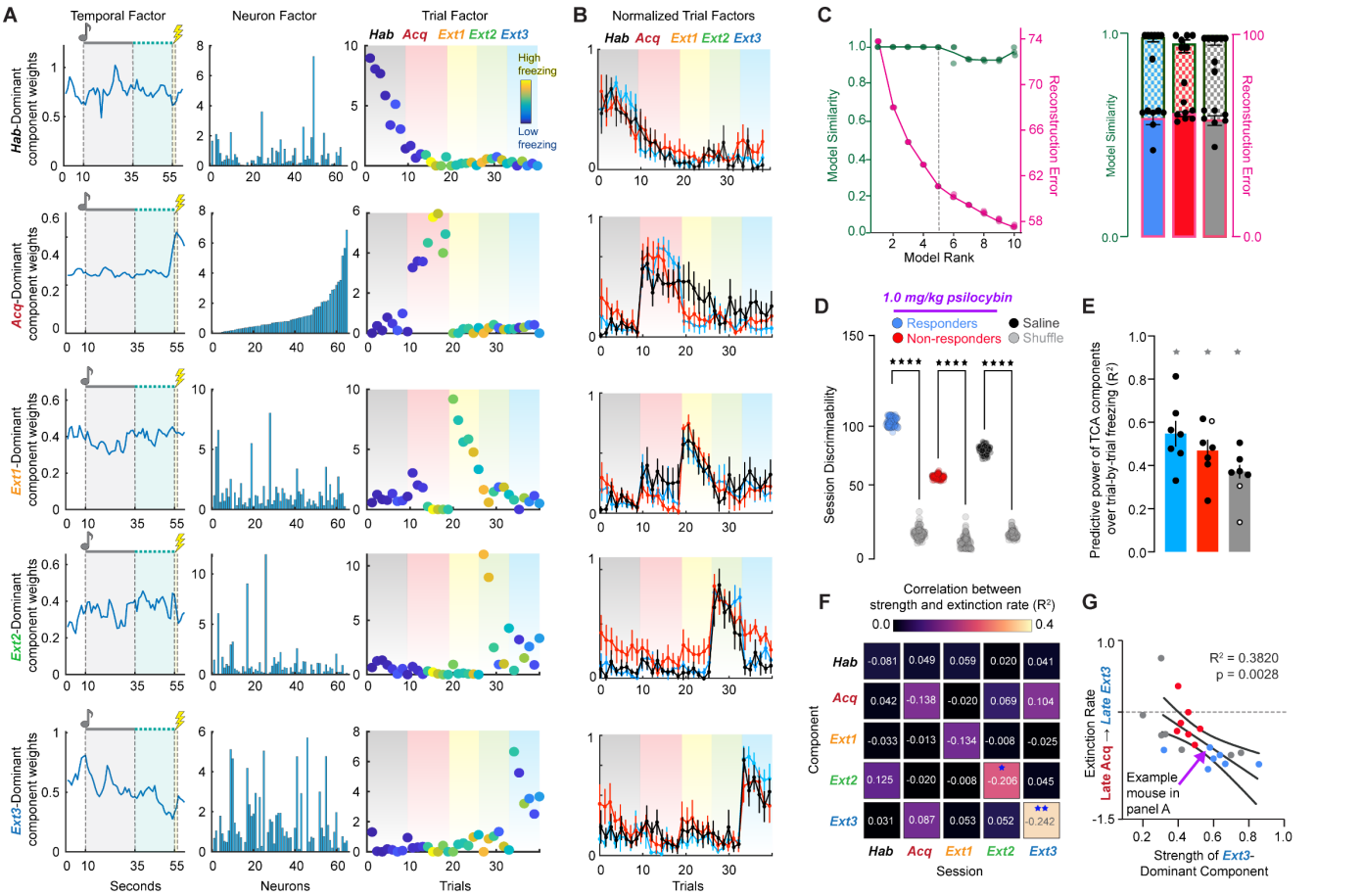

Figure 3 | TCA captures evolution of RSC through different task-relevant states over learning.
(A) Representative rank-5 TCA model of neural activity over RSC in one mouse. Rows correspond to unique components of neural activity and columns correspond to temporal, neuron, and trial factors. Values in each panel correspond to the factor loadings, or weights, of each component at each time, cell, and trial in the given component. Pink dashed line over temporal factors indicates time of conditioned one delivery, and lightning bolt indicates time of shock-delivery. Gradients over the trial factor indicate session of trials (Black = Habituation, Red = Acquisition, Yellow = Extinction 1, Green = Extinction 2, Blue = Extinction 3). Trial weights are color coded according to the animals % time freezing in each trial (dark blue = 0%, bright yellow = 100%). **(B)** Normalized trial factor weights for each component, averaged within groups. Two-Way RM ANOVA. (Supp. Table 1, rows 27-31). **(C)** Validation of choice of rank-5 model. Left: Four TCA models at each of ranks 1-10 were generated on neurons pooled from all psilocybin administered animals and their reconstruction error (pink) and model similarity (blue) plotted against each other. Rank-5 was chosen by minimizing reconstruction error while maximizing model similarity (black dashed line). (Supp. Table 1, row 32) Right: Reconstruction error (solid colors) and similarity (checkered colors) in individual animals. (Supp. Table 1, row 33) Ordinary One-Way ANOVA with Tukey multiple comparisons correction. **(D)** Trial weights of dominant factor during a given session divided by those of each other factor, summed over sessions, calculated over 100 iterations of TCA on real data from each group and TCA models generated on 100 shuffles of the data. Data was shuffled over cells at each individual timepoint to preserve all temporal and trial dynamics of activity that could lead to session discriminability. Multiple unpaired t-tests. P<0.0001 for all comparisons. (Supp. Table 1, row 34). **(E)** Linear regression trial factor value of each of 5 components and trial-by-trial freezing across all 5 days (R^2). Significant values are filled and non-significant values are hollow. Wilcoxon rank-sum. (Supp. Table 1, rows 35-36). **(F)** Linear regression of relative strength of each component during each session and extinction rate in all mice (R^2). Numbers are linear coefficients. Stars indicate where slope is significantly non-zero. (Supp. Table 1, row 37-41). **(G)** Data in D for the Extinction 3-dominant component during Extinction 3. (Supp. Table 1, rows 42). * p ≤ 0.05, ** p < 0.01, *** p < 0.001, **** p < 0.0001

treatment group. Data was arranged in into tensors t_{sec} x c_{cells} x T_{trials} in size. Model reconstruction error and similarity were plotted as a function of increasing model rank. The elbow method revealed that models of rank 5 were most appropriate for subsequent analysis (**Fig. 3C left**). Models of rank 5 were then generated for each animal (**Fig. 3C right**). Across animals, rank 5 models did not identify within-trial temporal dynamics beyond shock-responsiveness. (**Supp. Fig. 3A-E**) They did, however, cluster trials from the same session, suggesting that distinct RSC dynamics drive different phases of TFC acquisition and extinction across days (**Fig. 3A & B**). TCA thus extracted components of neural activity that dominated particular phases of learning.

To eliminate the possibility that the separability of sessions via TCA was due to changes in recording quality between days, 100 iterations of TCA on the real data from each group were compared to TCA models of 100 shuffles of the neural activity. Neural activity was shuffled by cells at each timepoint, such that the average activity over time and trials was preserved. The new neural activity tensors were thus t_{sec} x c_{shuff} x T_{trials}. This way, differences in recording quality between trials of different sessions and the within-trial temporal dynamics of the whole population, would be entirely conserved, but the ensembles driving those differences would be abolished.

To calculate the session discriminability of the real and shuffled TCA models, we exploited the clustering of trial factor weights within a given session, yielding a dominant component for each session. In a model of rank R, for component r in session s with mean trial weights $\overline{w}$, the relative strength of each component and the model's subsequent session discriminability index were calculated as:

$$Strength_{r,s} = \frac{\overline{w}_{r,s}}{\sum_1^R \overline{w}_{r,s}}$$

$$Session\ discriminability = \sum_1^S \max(Strength_s)$$

When cells were shuffled, session discriminability was significantly diminished in every group (**Fig. 3D, Supp. Table 1**). This result rejects the hypothesis that changes in RSC dynamics between sessions are due to recording artifacts and suggests that TCA identified genuine neural dynamics distinguishing sessions.

We also performed this analysis in non-shock control mice, who did not undergo any associative learning beyond neutral sensory integration and context familiarization (*i.e.,* no electric shocks during Day 2 *Acquisition*; **Supp. Fig. 5A, B, Supp. Table 1**). When neurons in the TFC conditioned psilocybin and saline groups were randomly subsampled to match the number of neurons recorded in non-shock mice, session discriminability was still significantly greater in all conditioned groups compared to non-shock mice (**Supp. Fig. 5C, D, Supp. Table 1**). This result confirms that the evolution through unique dynamics across days is a learning-related process in the RSC.

Relative strength of the *Extinction 3*-dominant component predicts extinction rate in psilocybin-administered mice.

If the evolution of neural activity through these session-dominating components over trials is linked to TFC extinction, the relative strength of the *Extinction 3*-dominant component compared to the others during *Extinction 3* within animals should predict extinction rate. Indeed, linear models comprised of each of the 5 components for each mouse as predictors strongly predicted freezing in all groups and almost all mice (**Fig. 3E, Supp. Table 1**). The relative strength of the component dominating each session after *Habituation* in its own session tended to be predictive of extinction rate with $R^2 > 0.1$, suggesting that the predominance of a unique component within a given session is related to extinction learning (**Fig. 3F, Supp. Table 1**). Importantly, while the strength of the *Acquisition*-dominant component during Acquisition positively predicts extinction rate, its strength during Extinction 3 negatively predicts it, supporting the observation from Figure 1 that differences in extinction rate are not due to stunted fear learning (**Fig. 3F, Supp. Table 1**). Finally, the *Extinction 3*-dominant component strongly and positively predicted extinction rate across groups, suggesting the identification of fear extinction related neural dynamics in the RSC by TCA. (**Fig. 3G, Supp. Table 1**).

Psilocybin induces turnover in the dominant neural ensembles driving RSC dynamics during TFC extinction.

As TCA returns the nonnegative weights of each temporal unit, neuron, and trial in each component, the neuron factor weights were used to identify ensembles driving the *Acquisition*-, *Extinction 1*-, and *Extinction 3*-dominant components of RSC activity in each mouse. When simulated tensors for each animal populated with identically behaving neurons, the mean and median weights were w = 1.0694 and 1.0709 respectively, suggesting that, if all neurons contributed equally neural dynamics, each neuron would be assigned w ~1 (**Supp. Fig. 6D-G**). Thus, w=1 was considered a reasonable null hypothesis for the strength of a neuron's participation in a given component, such that if a neuron's weight was greater than 1, then it was included in the ensemble (**Fig. 4A**).

All neurons with w>1 in the *Acquisition*-, *Extinction 1*-, and *Extinction 3*-dominant component are hereon referred to as the *Acq*-dominant, *Ext1*-dominat, or *Ext3*-dominant ensembles, respectively. This threshold achieves an average of ~40% of neurons included in each component's ensemble (**Fig. 4A**). Ensembles displayed considerable overlap at this threshold (**Fig. 4B, Supp. Fig. 4A-C, Supp. Table 1**). Ensemble overlaps are of interest as cells driving RSC dynamics on both *Acquisition* and *Extinction 1*, for instance, might in part comprise a neural substrate for a fear memory[61].

Overlaps in these ensembles significantly differed between psilocybin and saline mice in all cases, but not between responders and non-responders (**Fig. 4B, Supp. Table 1**). While 77% of *Acq*- and *Ext1*-dominant neurons are

identical on average in saline mice (*Acq/Ext1* and *Acq/Ext1/Ext3* neurons), this overlap was lower (48%) in both psilocybin groups, resulting in a greater proportion of *Acq-Only* neurons (**Fig. 4B top, Supp. Fig. 4A**). Similarly, the proportion of *Acquisition*-recruited neurons – *Acq/Ext1* and *Acq/Ext1/Ext3* – to *Extinction 1*-recruited neurons – *Ext1-*

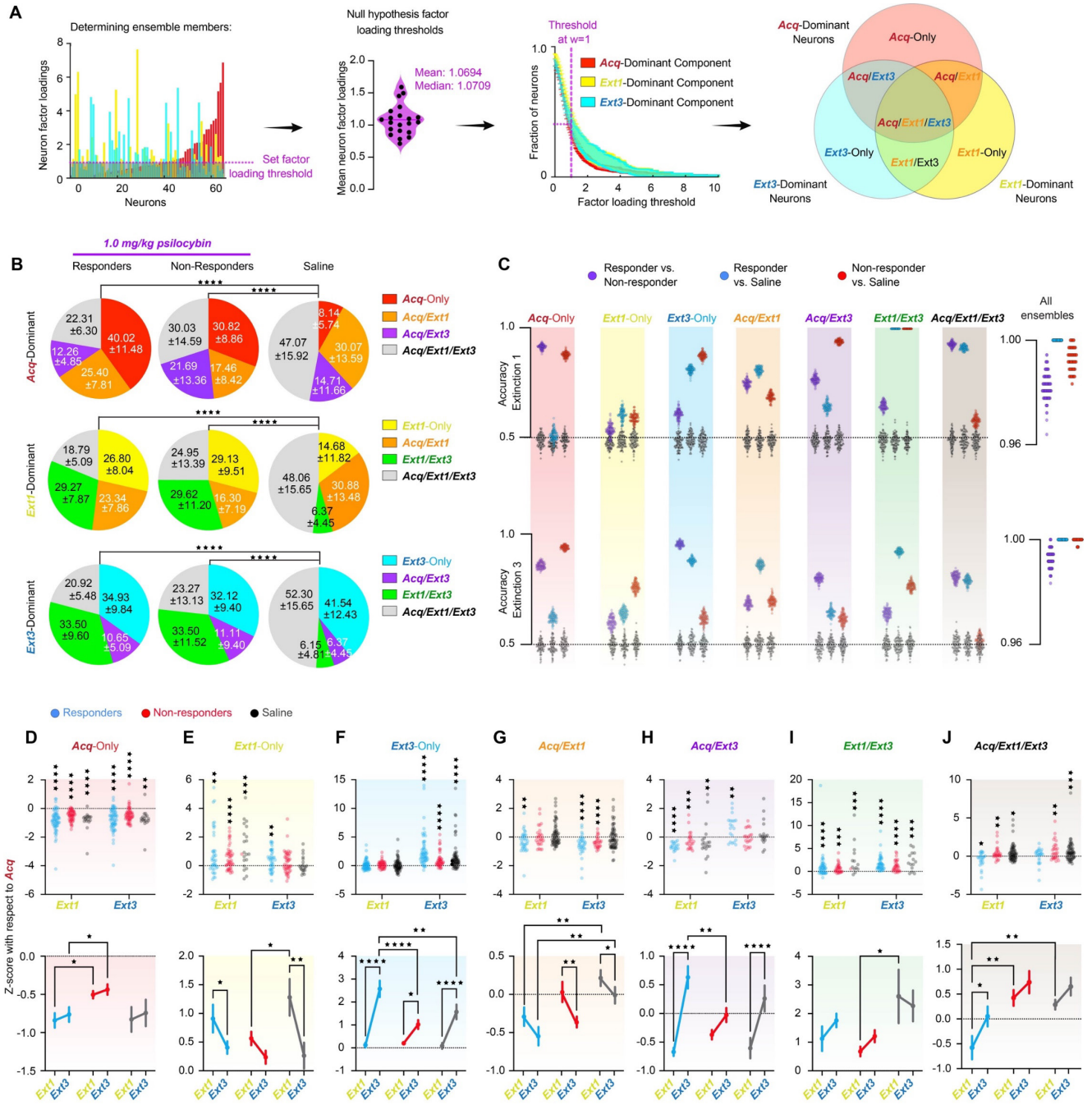

Figure 4 | Psilocybin bidirectionally modulates neural ensembles driving RSC dynamics during TFC in responders.
(A) Choosing Acq-, Ext1-, and Ext3-dominant neurons (red, yellow, and blue, respectively). Left: The fraction of neurons included in the ensemble at various thresholds across animals (mean, SEM) and the neuron factor weights of each neuron in each component in a representative animal. Neurons crossing the chosen threshold of *w=1* are indicated by enhanced opacity. Middle: Schematic of the overlaps between these neurons, yielding Acq-Only, Acq/Ext1, Ext1-Only, Ext1/Ext3, Ext3-Only, Acq/Ext3, and Acq/Ext1/Ext3. Ensembles are denoted by the corresponding ROYGBIV color code throughout the figure. Right: Example traces. **(B)** Pie charts describing the average overlap of the Acq-, Ext1, and Ext3-dominant ensembles (top, middle, bottom) in responders, non-responders and saline-administered mice. Numbers are mean ± SEM. Stars indicate comparisons between each psilocybin group and saline. Chi-square test. (Supp. Table 1, rows 43-45). **(C)** Accuracies of 100 Fisher decoders trained to predict responder status (left cloud, purple), responders from saline-administered mice (middle cloud, blue around grey), and non-responders from saline administered mice (right cloud, red around grey). Grey clouds are the same decoders tested on shuffled class labels. Decoders were trained on activity during Extinction 1 (top) and Extinction 3 (bottom). Right-hand panels accuracies of decoders trained on all seven ensembles as predictors. **(D)** Top: z-score activity in individual Acq-Only neurons in each ensemble from Acquisition. Wilcoxon rank-sum to test if change is different from zero. Bottom: Same data displayed as mean ± SEM. Two-way RM ANOVA to compare changes over time and between groups. (Supp. Table 1, rows 46-47). **(E-K)** Same as D) for Ext1-Only, Ext3-Only, Acq/Ext1, Ext1/Ext3, Acq/Ext3, and Acq/Ext1/Ext3, respectively. (Supp. Table 1, rows 48-59). * p ≤ 0.05, ** p < 0.01, *** p < 0.001, **** p < 0.0001

Only and *Ext1/Ext3* – is much lower in psilocybin mice than saline mice, ~41/59% as opposed to 79/21% (**Fig. 4B middle, Supp. Fig. 4B, Supp. Table 1**). Subsequently, about 30% of new, *Extinction 1*-recruited neurons proceeded to join the *Ext3*-dominant ensemble in both responders and non-responders, in contrast to only 6% of *Ext1*-dominant neurons in saline mice (*Ext1/Ext3* neurons) (**Fig. 4B middle, Supp. Fig. 4B, Supp. Table 1).** Finally, similar proportions (30-40%) of neurons were newly recruited during *Extinction 3* in all groups (**Fig. 4B bottom, Supp. Fig. 4C, Supp. Table 1**). However, only 6% of *Ext3*-dominant neurons were newly recruited in *Extinction 1*, leaving a remaining 58% of *Ext3*-dominant neurons overlapping with the with the *Acq*-dominant ensemble (6% *Acq/Ext3* and 52% *Acq/Ext1/Ext3*). In psilocybin mice, an average of about 34% of *Ext3*-dominant neurons were *Ext1/Ext3* neurons, while only 32-34% of neurons were shared with the *Acq*-dominant ensemble. Thus, psilocybin accelerates a rapid turnover from fear acquisition-dominating neurons to a novel population, which subsequently drives RSC activity persistently throughout extinction training. This result is highly consistent with the hypothesis that psilocybin both establishes and stabilizes novel ensembles underlying behavioral flexibility.

Non-shock controls also displayed significantly different distributions of overlaps compared to saline mice (**Supp. Fig. 5E-G, Supp. Table 1**). In non-shock controls, the proportion of *Acq*-dominant neurons overlapping with *Ext1*-dominant neurons was much smaller than in saline mice, while the overlaps between *Ext1*-dominant neurons and *Ext3*-dominant neurons were much greater. These result supports the hypothesis that preferential overlaps of *Acq/Ext1-* and *Ext1/Ext3*-dominant ensembles, in saline and psilocybin mice respectively, indicate enhanced stability of behaviorally relevant fear acquisition- and extinction-related ensembles over time.

Activity in neural ensembles predicts treatment and responder status.

Fisher linear decoders were trained to distinguish between psilocybin responders, non-responders, or saline-treated mice based on the average activities of each identified ensemble during either *Extinction 1* or *Extinction 3* (**Fig. 4C, Supp. Fig. 4**). All models were trained on 50% of the dataset and tested on the other 50%. Decoders were trained to classify two groups at a time – responders vs. non-responders (purple), responders vs. saline (blue), non-responders vs. saline mice (red). If a given decoder can distinguish treatment (psilocybin or saline) both blue and red distibutions should be non-overlapping with a shuffle distribution (grey). If this decoder can distinguish psilocybin responsiveness, the purple distribution should not overlap with the shuffled distribution.

During *Extinction 1*, when psilocybin mice were under acute influence of the drug, the *Ext3-Only* and *Ext1/Ext3* ensembles significantly distinguished both groups of psilocybin mice from saline mice, suggesting that psilocybin affected activity in these ensembles in a manner specific to its acute pharmacological actions but not to its future impacts on behavior (**Fig. 4C top**). On the other hand, the *Acq/Ext1* ensemble significantly discriminated between all groups, suggesting that psilocybin indeed modulated these neurons, but differently in responders than in non-responders. This result suggests that psilocybin's acute effects on task-relevant neurons can differ across animals acutely in a manner that predicts future behavioral change. The *Acq/Ext1/Ext3* ensemble significantly discriminated between responders and the other two groups, but not between non-responders and saline mice, suggesting that, while this ensemble is not determinately effected by psilocybin alone, altered activity in this ensemble during psilocybin administration may enhance future behavioral change. Conversely, the *Acq-Only* and *Acq/Ext3* ensembles significantly distinguished non-responders from the other two groups, suggesting that altered activity in these ensembles during psilocybin administration may impair future behavioral change.

During *Extinction 3*, most ensembles preserved their predictive ability, in terms of which groups were differentiable based on their activity, with the exception of the *Acq/Ext3* and *Ext3-Only* ensembles (**Fig. 4C bottom**). The *Acq/Ext3* ensemble distinguished between responders and non-responders, but not non-responders and saline mice as it did during *Extinction 1*. This result suggests that non-responders proceed to exhibit saline-like dynamics in *Acq/Ext3* neurons in *Extinction 3*, while responders persistently display altered dynamics in this group of neurons. Similarly, the *Ext3-Only* ensemble had differentiated between psilocybin and saline mice during *Extinction 1*, but in *Extinction 3* comes to differentiate responders from the other two groups instead. This result suggests that psilocybin acutely alters dynamics in these neurons during *Extinction 1*, but persistent alterations in these dynamics in *Extinction 3* accompany the enhanced extinction rate observed in psilocybin responders.

When models were trained on all seven ensembles as predictors, they predicted treatment and responder status with > 95% accuracy on all 100 iterations for each pair (**Fig. 4C right**). The ability of many ensembles to distinguish responder status during *Extinction 1* suggests that neural activity in the RSC during psilocybin exposure may be a crucial determinant of therapeutic-like response 48 hours later.

Psilocybin suppresses *Acq*-dominant neurons and potentiates *Ext3*-dominant neurons in responders.

To explore the development of the distinctive predictive characteristics of each ensemble, we calculated how the activity of each neuron in these ensembles changed from the *Acquisition* session.

Acq-Only neurons were suppressed during *Extinction 1* and *Extinction 3* in all groups, but significantly less so in non-responders (**Fig. 4D, Supp. Table 1**). As the *Acq-Only* ensemble distinguished non-responders from responders and saline mice, during both *Extinction 1* and *Extinction 3*, this result suggests that suppression of *Acq-Only* neurons in future sessions is an endogenous characteristic of TFC extinction in mice that may have been impaired or slowed by psilocybin in non-responders.

Ext1-Only neurons were potentiated in all groups during *Extinction 1*, but only remained significantly greater than zero during *Extinction 3* in responders (**Fig. 4E, Supp. Table 1**). However, this ensemble had limited predictive abilities regarding both responsiveness and treatment, weakening the claim that this difference is crucial for psilocybin's effects on TFC extinction.

Ext3-Only neurons were strongly recruited in all groups in *Extinction 3*, but significantly more greatly in responders (**Fig. 4F, Supp. Table 1**). Curiously, there is no difference in the activity of this ensemble between groups during Extinction 1 (**Fig. 4C**), raising the question of what features of this ensemble distinguished psilocybin from saline animals at this time. Nevertheless, that the *Ext3-Only* ensemble significantly distinguished between responders from the other two groups in *Extinction 3* suggests that this enhanced activation of *Ext3-Only* neurons 48 hours after drug administration may drive enhanced TFC extinction in responders.

Acq/Ext1 neurons were significantly suppressed during *Extinction 1* in responders, while it was unchanged in the other groups. In responders, *Acq/Ext1*-dominant neurons were persistently suppressed during *Extinction 1* and *Extinction 3* compared to *Acquisition* (**Fig. 4G, Supp. Table 1**). In contrast, these neurons maintained their activity during *Extinction 1* in non-responders before being suppressed, and were maintained throughout in controls, likely underlying this ensembles' ability to distinguish between all three groups. This result suggests that, although psilocybin results in the suppression of *Acq/Ext1* neurons 48 hrs after drug administration in both responders and non-responders, it may only ultimately enhance extinction when *Acq/Ext1*-dominant neurons are suppressed during acute drug effects.

The *Acq/Ext3*-dominant ensemble was significantly suppressed in *Extinction 1* in all animals, and subsequently strongly potentiated with respect to *Acquisition* levels in *Extinction 3* in responders and saline controls, suggesting that these neurons were suppressed during acute drug effects and subsequently re-recruited in responders (**Fig. 4H, Supp. Table 1**). Likewise, the *Ext1/Ext3*-dominant ensemble was potentiated across days with respect to *Acquisition* in all groups (**Fig. 4I, Supp. Table 1**).

Finally, the *Acq/Ext1/Ext3* ensemble driving activity in all three sessions was suppressed during *Extinction 1* in responders but potentiated in non-responders and saline mice (**Fig. 4J, Supp. Table 1**). This result suggests that acute suppression of this ensemble during psilocybin administration may enhance the likelihood of enhanced TFC extinction.

Here, a pattern emerges. In responders, all ensembles driving activity during *Acquisition* are suppressed during *Extinction 1* whereas *Acq/Ext1* and *Acq/Ext1/Ext3* ensembles are either maintained or potentiated during *Extinction 1* in non-responders. Meanwhile, neurons recruited after *Extinction 1* are more strongly active in responders than non-responders.

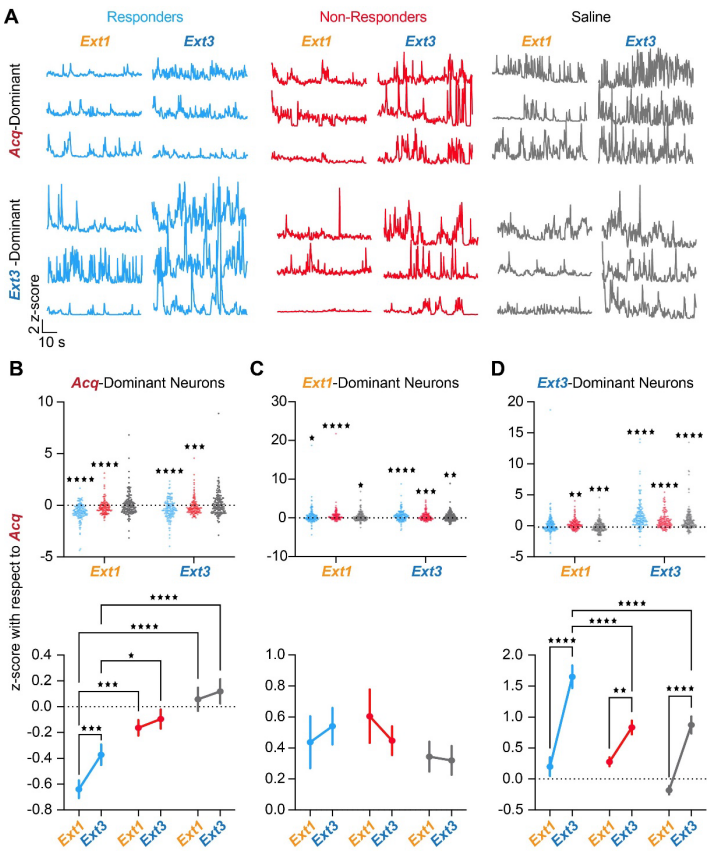

Figure 5 | Psilocybin induces long-term suppression of *Acq*-dominant neurons and strong post-acute recruitment of *Ext3*-dominant neurons in responders.
(A) Example traces of Acq-dominant (top) and Ext3-dominant (bottom) neurons during Extinction 1, and Extinction 3 in each group. **(B)** Top: z-score with respect to Acquisition of individual Acq-dominant neurons in each ensemble during Extinction 1 and 3. Wilcoxon rank-sum to test if median ≠ 0. Bottom: Same data displayed as mean ± SEM. Two-way RM ANOVA to compare changes over time and between groups. (Supp. Table 1, rows 60-61). **(C)** Same as B) for Ext1-dominant neurons. (Supp. Table 1, rows 62-63). **(D)** Same as B) for Ext3-dominant neurons. Table 1, rows 64-65). Data are represented as mean ± SEM. * $p \leq 0.05$, ** $p < 0.01$, *** $p < 0.001$, **** $p < 0.0001$.

For a holistic picture of these results, one can consider the entire *Acq*-, *Ext1*-, and *Ext3*-dominant ensembles. In saline mice, which maintain *Acquisition*-like freezing levels throughout *Extinction*, the *Acq*-dominant ensemble is similarly persistently active at *Acquisition*-like levels throughout *Extinction* (**Fig. 5B, Supp. Table 1**). This result is specific to TFC-trained mice, as opposed to non-shock mice, indicating the persistence of a potential substrate for fear memory throughout extinction in saline mice (**Supp. Fig. 5H, Supp. Table 1**). In contrast, psilocybin persistently suppresses the *Acq*-dominant ensemble, strongly in responders and weakly in non-responders (**Fig. 5B, Supp. Table 1).** The *Ext1*-dominant ensemble is potentiated throughout extinction in all groups (**Fig. 5C, Supp. Fig. 5I, Supp. Table 1**). Finally, great recruitment of the *Ext3*-dominant ensemble occurred in all TFC-trained mice and more greatly in saline mice than non-shock controls, suggesting that heightened activity in novel RSC ensembles is a feature of TFC extinction (**Fig. 5C, Supp. Fig. 5J, Supp. Table 1**). However, the *Ext3*-dominant ensem-

ble is most strongly recruited in psilocybin responders compared to any other group. Critically, these results were highly robust to varying the factor loading thresholds determining a neuron's ensemble membership (**Supp. Fig. 6A-C, H**). Thus, psilocybin enhances TFC extinction in animals by bidirectionally modulating ensembles underlying different phases of TFC.

Discussion.

In this study, we combined *in*-vivo single cell calcium imaging of cortical ensembles with behavioral pharmacology to elucidate the neural correlates of psilocybin-enhanced extinction. Here, we report for the first time that mice are divided into psilocybin-responsive and -non-responsive groups with respect to post-acute enhancement of TFC. In drug-responsive animals, psilocybin acutely suppresses expression of the fear memory and subsequently enhances expression of extinction 24 and 48 hours later. In non-responsive animals, psilocybin has no effect on behavior compared to extinction rate-matched saline animals. While psilocybin neither altered neural responses in the RSC to within-trial stimuli nor freezing encoding, psilocybin treatment was associated with robust bidirectional modulation of RSC ensembles dominating various phases of fear acquisition and extinction in responders.

We repeated the above behavioral pharmacology experiment while imaging large-scale RSC ensembles within male mice and found similar psilocybin-responsiveness, using our empirically validated extinction rate threshold (-50% freezing/3 days). Many RSC neurons exhibited tone, trace, and shock-responsiveness. However, most neurons failed to maintain their particular response properties over days, suggesting a lack of stability of within-trial dynamics over time. If there are stable representations of discrete sensory events in the RSC, this evidence suggests they are unlikely to follow a labeled-line code and may be subject to great representational drift, reported previously[80]. Interestingly, about half of all tone-responsive neurons were also trace-responsive on any given day, consistent with studies showing persistent encoding of cue value in the RSC throughout whole trials[53,54]. Thus, though the neural correlates of within-trial events vary greatly across cognitive and behavioral context, they do not vary so much within that same context. We therefore concluded that across-trial, rather than within-trial, dynamics may be the more crucial signal.

We used TCA to identify trial-varying components of neural activity associated with fear extinction and putative task-relevant ensembles[78]. Consistent with the hypothesis that the RSC preferentially encodes the cognitive or behavioral context associated with sensory events as opposed to the sensory events themselves, the trial factor weights of these components tended to cluster trials from the same session without clear organization of the temporal factor weights across animals. We not only found that this session-discriminability was significantly greater in TCA models trained on real data compared to shuffled data across groups, eliminating the possibility that these observations were due to changes in recording quality between sessions, but also that session discriminability was significantly reduced in non-shock controls. The non-shock control is appropriate here because the RSC is also involved in contextual fear conditioning and may therefore exhibit similar neural correlates in both paired and unpaired conditioning protocols[50,61,68,69]. Non-shock controls thus permit the broad isolation of fear acquisition- and extinction-related signals from those associated with neutral contextual novelty, exploration, and integration [47-49,52,56,57,76]. We further found that the strength of the *Ext3*-dominant component most strongly predicted extinction rate in conditioned mice, suggesting that the predominance of this component over others is associated with extinction learning. We therefore concluded that TCA successfully extracted task-relevant dynamics from RSC activity.

We chose to more closely examine the *Acq*-, *Ext1*-, and *Ext3*-dominant ensembles due to the cognitive and behavioral significance of those sessions. During *Acquisition*, the animals are under acute threat, encoding the fear memory. During *Extinction 1*, animals are simultaneously recalling fear, extinguishing fear, and undergoing acute drug treatment. Finally, during *Extinction 3*, responders emerge and express robust extinction. Using the neuron factor weights in each component, we identified the neural ensembles driving dynamics represented by each factor and designated them the "*Acq*-, *Ext1*-, or *Ext3*-dominant" ensembles. The extent of overlaps in these ensembles bestows the advantage of identifying putative memory ensembles. For instance, neurons classified as both *Acq*- and *Ext1*-dominant might constitute a candidate substrate for fear memory, whereas neurons classified as both *Ext1*- and *Ext3*-dominant might constitute a candidate substrate for extinction memory. That Fisher decoders trained on each ensemble could accurately distinguish responders, non-responders, and saline mice indicates their relevance to psilocybin's acute and post-acute effects.

Since the RSC is necessary for TFC, we expected to find a high proportion of overlapping *Acq/Ext1* and *Acq/Ext1/Ext3* neurons in saline controls as previously observed[61], and we did. Intriguingly, psilocybin substantially reduced this proportion in responders and non-responders. It was shown elsewhere that unconditioned freezing can be evoked in a novel context by optogenetically reactivating RSC-tagged neurons that were initially active during fear learning in another context (i.e., akin to the *Acquisition* session responsive cells)[61], raising the possibility that *Acq/Ext1* and *Acq/Ext1/Ext3* ensembles may be participating in encoding the fear memory. This reduction in putative "fear memory" neurons in psilocybin mice resulted in a four to five-fold increase in *Acq-Only* neurons, suggesting that psilocybin induced a robust turnover in the composition of the ensembles driving RSC activity in the *Extinction 1* session. We found that these *Acq-Only* neurons strongly decreased their activity during *Extinction 1* in all groups; however, this effect is significantly greater in responders than non-responders. As responders had about twice the proportion of *Acq-Only* neurons than saline mice, this contributes to a significantly greater net inhibition of *Acq*-dominant neurons in responders than controls. This greater net-decrease was

exacerbated by the simultaneous suppression of *Acq/Ext1* and *Acq/Ext1/Ext3* neurons during the *Extinction 1* session, while these neurons maintain or even surpass *Acquisition*-like levels of activity throughout training in saline controls.

In non-shock control mice, neurons that were dominant during Day 2 – in other words, neurons that were dominant in Context B – decreased their activity during Days 3 and 5 – in Context A – indicating the presence of context discrimination in RSC neurons of un-conditioned mice. By contrast, the persistent activation and stability of the *Acq*-dominant ensemble in conditioned saline mice must be a consequence of fear conditioning, abolished by psilocybin. All told, while a large proportion of *Acq*-dominant neurons persistently maintained their activity during *Extinction 1* in controls, as expected during a fear-recall session, these neurons were suppressed during *Extinction 1* in psilocybin responders.

In psilocybin non-responders, the *Acq*-dominant neurons that overlap with *Ext1*- and *Ext3*-dominant ensembles tended to be more weakly suppressed, maintained or even potentiated during *Extinction 1*. Indeed, the activity of every *Acq*-dominant ensemble during *Extinction 1* predicted responder status. The discrepancy between responders and non-responders raises the possibility that the concurrent activation of *Acq*-dominant neurons during *Extinction 1* alongside psilocybin administration might prevent or slow psilocybin's therapeutic-like effects on fear extinction. Whether psilocybin is *inducing* inhibition in these neurons in responders or psilocybin's actions merely co-occur with heightened suppression of this ensemble is an open question.

It has been previously shown that novel ensembles are recruited in the RSC during fear extinction[61,73]. Indeed, we observed a substantial recruitment of neurons unique to the *Ext3*-dominant ensemble in all groups, with significantly lesser activation in non-shock mice. In psilocybin responders, these neurons were significantly more strongly activated during *Extinction 3* than non-responders and saline controls, about twice as strongly as either of the other groups. This increase in activation was driven by uniquely strong increases in *Ext3-Only* and *Acq/Ext3* neurons. Interestingly, psilocybin also increased the proportion of *Ext1/Ext3* neurons. While psilocybin- and saline-administered mice ultimately recruit very similar proportions of *Ext3*-dominant neurons after *Acquisition*, in controls, these neurons are primarily composed of *Ext3-Only* neurons rather than *Ext1/Ext3* neurons. In controls, the substantial ensemble turnover occurs sometime between *Extinction 1* and *3*; however, in psilocybin mice, this turnover is accelerated and occurs earlier, between *Acquisition* and *Extinction 1* instead. This conclusion is supported by the fact that *Ext3*-dominant neurons were suppressed during *Extinction 1* in saline administered mice alone, indicating a possible increase in activity in this set of neurons coinciding with psilocybin administration. Thus, neurons acutely recruited by psilocybin go on to form a stable ensemble that continues to be potentiated later in extinction. This interpretation is in agreement with dendritic and synaptic plasticity studies that demonstrate psilocybin rapidly induces the formation and subsequent long-term stabilization of behaviorally relevant neural pathways.

Given the reported half-life of psilocin is ~117 min in rats, the enhanced activation of *Ext3-Only* neurons in psilocybin responders during *Extinction 3*, but not *Extinction 1*, suggests that this is a post-acute consequence of psilocybin days after the compound has cleared the body. What latent variables confer psilocybin responder statues (*e.g.,* genetic, circuit connectivity, environment, etc.) remains unclear at this time. Encouragingly however, optogenetic studies in which extinction recruited RSC neurons were genetically captured and activated after fear re-conditioning demonstrated that the activation of these neurons was sufficient to reinstate extinction[61]. Together, this evidence suggests that the enhanced activation of these neurons after psilocybin administration in mice may in fact represent enhanced extinction learning and/or expression. Future experiments will need to verify this claim.

These results have important implications for future preclinical research on psychedelics. For instance, the canonical mechanism for psychedelic-induced, therapeutically relevant effects in preclinical studies is the excitation and subsequent neural plasticity induced downstream of 5HT2ARs[81]. Indeed, several of our results suggest that this type of plasticity may likely be associated with psilocybin enhanced fear extinction, via the rapid recruitment of the *Ext1/Ext3* ensemble and enhancement of activity in the *Ext3-dominant* ensemble. However, the mechanism for the suppression of fear-associated neurons during psilocybin administration observed here, which greatly distinguished responders from non-responders and controls, is unknown.

Although psilocybin induces inhibitory effects in many subcortical regions via 5HT1Rs, direct psychedelic-induced cellular inhibition in cortical neurons was reported for the first time recently[82]. This suppression of *Acq*-dominant neurons in psilocybin responders echoes recent findings that inhibitory plasticity in fear memory engrams in the hippocampus is necessary for the development memory selectivity, measured by the relative reduction of freezing in neutral contexts over time[83]. Perhaps psilocybin invokes a similar mechanism to accelerate extinction learning. Still, since suppression of *Acq-dominant* neurons occurred most robustly in the drug-responsive subpopulation of mice, it would seem this phenomenon is not a guaranteed effect of psilocybin but could be critical for positive behavioral outcomes. Indeed, a single-dose of psilocin reduces neural activities to aversive airpuffs in central amygdalar cells days later, hinting that weakened neural activities within negative valence-encoding circuits may partially contribute to this observation[84]. How is this ensemble targeted for suppression in this group of mice? Is its suppression somehow important for the enhanced recruitment of extinction-associated ensembles? How do genetic predispositions, set, and setting affect the likelihood of this outcome? Answers to these questions, we may be able to greatly enhance the safety and efficacy of psilocybin-assisted therapy by determining individualized treatment programs.

One important limitation of this study is the lack of cell-type specificity of imaged neurons. Principal cells and various kinds of inhibitory interneurons form a complex microciruitry in cortex and carry out unique computational functions. Still, as a first glance into the impact of psilocybin on single neurons in mice undergoing TFC extinction, our non-specific approach afforded the benefit of identifying functional subpopulations that can be genetically dissected in the future. For instance, psilocybin engages multiple 5HT receptor subtypes, and intriguingly the RSC is unique from the rest of cortex due to the fact that it expresses a dense population of 5HT2CR-containing excitatory neurons and lower levels of 5HT2ARs[66]. Perhaps these differential 5HT receptor-expressing neurons comprise one or more of the functional ensembles identified here.

Taken together, these results suggest that psilocybin both enhances endogenous mechanisms of fear extinction – the potentiation of newly recruited RSC neurons – and engages non-typical mechanisms as well – the suppression of fear acquisition-dominating neurons in drug responders. These results support a current field hypothesis that the neurophysiological effects of psychedelics underlying behavioral flexibility involve altering task-relevant activity in neural ensembles over subsequent days[84]. However, rather than simply accelerating or enhancing endogenous mechanisms of cognitive flexibility (*i.e.,* increasing activity in new ensembles), psilocybin also engages a neural ensemble-level inhibitory mechanism of fear extinction. Indeed, the acute, response-predicting effects of psilocybin observed in this study are entirely comprised of inhibition of fear acquisition-associated neurons. Psilocybin's enhancement of extinction-like activity is not observed until the days following treatment. This result raises the possibility that psilocybin's acute suppression of fear acquisition-associated neurons supports the future recruitment of extinction-associated neurons. Future research will explore how the neuroplastic effects of psilocybin on a cellular and circuit level evoke these distinct effects on neural dynamics and establish a causal relationship between the ensemble-specific changes in activity observed here with behavior.

Methods.

Experimental Methods.

Animals: Animals used in all studies were C57BL/6J mice from Jackson Laboratories (RRID: IMSR_JAX:000664). Mice were kept on a reverse 12 hour light/dark cycle. Behavior was performed at least 1 hour and no more than 4 hours following lights-off. Group-housed males (n=34) and females (n=16) between 8-12 weeks of age were used in the behavioral pharmacology experiment in Fig. 1. For the Miniscope study, males of 8-10 weeks of age underwent viral injection surgeries, followed by implantation of 4.0 (length) x 1.0mm (diameter) GRIN lens at 10-12 weeks, and behavior at 12-16 weeks (minimum 2-week recovery time from last surgery). Mice were singly housed following implant surgery.

TFC Conditioning and Extinction: One week prior to behavioral testing, Miniscope mice were habituated to the Miniscope for 2 days in 10 min sessions in the home cage. All mice underwent behavioral training and testing in Med Associates fear conditioning boxes for five days. In Context A, Med Associates chambers were equipped with smooth white floor inserts and cleaned with ethanol to provide a unique olfactory, tactile, and visual context. In Context B, the shock grid floor was exposed, mouse bedding was placed in a tray under the floor, and chambers were cleaned with Clidox. The five days of behavioral testing consisted of *Habituation* (Hab), *Acquisition* (Acq), and *Extinction 1-3* (Ext1-3). Hab and Ext1-3 took place in Context A, and *Acquisition* took place in Context B. The CS consisted of a 4kHz, 75dB tone delivered in 25, 200ms pips at 1Hz. During *Acquisition*, the CS was followed by a 20sec trace period preceding a 1mA, 2sec shock. On all other days, the shock was omitted. *Habituation* and *Acquisition* consisted of 8 trials, with jittered ITIs of 60±10sec. During *Extinction 1-3,* there were 6 trials per session. 30 minutes prior to *Extinction 1*, mice were injected with 1mg/kg psilocybin, contributed by the Elizabeth Heller Laboratory at the University of Pennsylvania, or saline. Mice were excluded from the study if they froze ≤20% of the time during *Acquisition* or ≤10% of the time during the first half of Extinction 1 (n=23 mice, Supp. Fig. 1D). Two mice were excluded due to excessive barbering in the home-cage during the days of the experiment.

For Miniscope studies, a 2"-diameter hole was drilled in the top of a Med Associates box to feed the cables through. During the sessions, recordings were remotely controlled and streamed to a laptop for live monitoring. Recordings were made at LED power (0.7-1.5mW), gain (1.0-3.0), and focus (0-300μm) settings deemed appropriate for each mouse and kept as consistent between recording days as possible.

For the non-shock control condition, Miniscope-implanted mice underwent an identical protocol, except for the total omission of the shock.

Surgery: For Miniscope studies, all mice were unilaterally injected with 800nL of AAV9-syn-GCaMP8m-WPRE at a titer of 1.2e12 (Addgene virus #162375) in the RSC. RSC coordinates were chosen from past studies: -2.25 AP, +0.3ML,-0.8 DV. Mice were anesthetized with isoflurane. Hair was removed with Nair, and the skin sterilized with Betadine and ethanol. An incision was made with scissors along the scalp. Tissue was cleared from the skull surface using an air blast. The skull was leveled such that the Bregma-Lambda and ML DV difference was within ±0.1mm. A craniotomy was made at the chosen coordinates with a dental drill. A needle was lowered to the target coordinates through the craniotomy and virus infused at 100nL/min. The needle was left in the brain 10mins after infusion before being slowly withdrawn. The incision was sutured, and the animal was administered Meloxicam before being placed under a heat lamp for recovery.

Miniscope implantation surgeries subsequently followed the same protocol until the craniotomy step. A 1mm craniotomy was made by slowly widening the craniotomy with the dental drill. Dura was peeled back using microscissors, sharp forceps, and curved forceps. The craniotomy was regularly flushed with saline, and gel foam was applied to absorb blood. An Inscopix Pro-View Integrated GRIN lens and baseplate system was attached to the Miniscope and a stereotax. Using the Inscopix stereotax attachment, the lens was slowly lowered into a position over the injection site. The final DV coordinate was determined by assessing the view through the Miniscope stream. If tissue architecture could be observed in full focus with light fluctuations associated with RSC slow oscillatory activity under anesthesia, the lens was implanted at that coordinate (-0.6 to -0.3DV). The GRIN lens + baseplate system was secured to the skull with Metabond and then dental cement. After surgery, mice were singly housed and injected with Meloxicam for three consecutive days during recovery.

Miniscope validation: Before admission to the experiment, the Minsicope was magnetically attached to each animal's implant for habituation and streamed using the Inscopix Data Acquisition Software. If many cells could be observed during spontaneous behavior in the home cage, the mouse was admitted. If only a few cells were visible, the session was recorded and analyzed in the Inscopix Data Processing Software (IDPS) to determine the number of observable cells. If an animal had >20 identifiable cells, they were admitted into the study. Others were euthanized.

Histology: Animals were perfused with 10% formalin and brains dissected. Brains were stored in formalin solution for 24 hours before being transferred to 30% sucrose. Brains were sectioned at 50µm on a cryostat and stored in PBS. RSC sections were stained with DAPI and sections from -2.18AP to -2.88AP were mounted on slides. The section with the deepest and widest GRIN lens track was designated as the coordinate of implant.

Analysis Methods.

Behavioral: Behavior was recorded by Basler cameras into Pylon Viewer at 15Hz. Videos were then processed in the open source ezTrack Jupyter Notebook. The algorithm was calibrated to the standard light fluctuations in the empty chambers and the empty chambers with the Miniscope wire dangling in them for each respective study. A freezing threshold was determined in terms of number of pixels changed/frame by visually validating portions of videos classified as "Freezing" or "Moving" by the algorithm. In general, a freezing threshold of 50-200pixels/frame was used in non-Miniscope studies, whereas a threshold of 300pixels/frame was used in all Miniscope animals, likely necessitated by movements of the Miniscope wire. An animal was only classified as "Freezing" if the pixels/frame remained below threshold for at least 1sec, or 15 frames. Freezing status per frame was exported in a CSV file and post-processed in Matlab to calculate % freezing in particular windows of time. Freezing plotted here is % freezing during the trace period, as this is the interval of time invoking the RSC for fear and extinction encoding and retrieval. Freezing videos were aligned to trial times by beginning analysis at the first frame of the red light in the Med Associates boxes switching on, indicating session start. Although tone delivery times were pseudo-random with respect to the animals, they were hard-coded by the experimenter, so analysis alignment to session start was sufficient to align video to tone.

Calcium imaging pre-processing: Videos were downloaded from the Inscopix Data Acquisition Box and uploaded to the Inscopix Data Processing Software (IDPS). Videos were spatially downsampled by a factor of 4 and spatial bandpass filtered between 0.005 and 0.500. Videos were then motion corrected with respect to their mean frame. Cells were identified and extracted using CNFM-E (default parameters in the Inscopix implementation of CNMF-E, except the minimum in-line pixel correlation = 0.7 and minimum signal to noise ratio = 7.0) and second-order deconvolved using SCS. Videos across 5 days of behavioral training were longitudinally registered in IDPS (minimum normalized cross-correlation = 0.1). Only cells registered on all 5 days were considered for further analysis.

Calcium imaging post-processing: The majority of subsequent analysis was performed in custom Matlab scripts, available in the associated Github. Deconvolved calcium traces of cells from each session were aligned according to their global cell index determined in longitudinal registration. As the window considered for each trial included a 10sec baseline period, a 25sec stim period, a 20 sec trace period, a 2 sec shock/omission period, and 3 sec after, each trial was 60sec. Neural activity was therefore summed within 1 sec time windows. Miniscope recordings were started exactly 30.00sec before behavioral session start, and this information was used to align data to behavior and neural data. To determine whether a cell was stim, trace, and/or shock responsive, their baseline period activity was compared to their activity during the time period of interest by Wilcoxon rank-sum. The proportion of stim/trace/shock-responsive cells compared to all cells recorded within an animal was calculated for each session and compared between groups and over time with a Two-Way RM ANOVA. To calculate the change of activity in groups of neurons between sessions, activity was z-scored to traces recorded in *Acquisition* and compared between groups and over time with a Two-Way RM ANOVA. To calculate overlaps between ensembles of neurons, ensembles were identified by TCA (described below) in each animal. Whether these overlaps were small or large was determined by a Wilcoxon rank-sum test comparing the median of each overlap in each group with a 50% threshold. If an ensemble shared significantly <50% of neurons with another, this was considered a small overlap.

Freezing encoding: To calculate freezing encoding in single neurons, neural traces were downsampled from 20 to 15Hz and aligned to a 15Hz binary freezing trace. A binomial GLM was trained on half of the data from each session and

tested on the other half to generate auROCs. The mean auROC of all neurons in a mouse in each session was reported in the main text.

TCA: To perform TCA, post-processed calcium imaging data was arranged into tensors t_{sec} x c_{cells} x T_{trials} in size for each animal, exported as a Matlab structure, and imported into Spyder where we employed the TensorTools package developed by Williams et al., 2018. To determine the appropriate model rank empirically, TCA was first run on the pooled and aligned tensors from all mice in a given treatment group, and model reconstruction error and similarity were plotted as a function of increasing model rank. The elbow method revealed that models of rank 5 were most appropriate for subsequent analysis (Reconstruction error = 0.615; Model similarity between four iterations = 1). Models of rank 5 were then generated for each animal.

In order to measure the dominance of each of the 5 components during a given trial, the relative strength of a given component was measured as the fraction of the total trial weights at that time assigned to that given component. This measure functions as a way to assess how dominant this component is over others at a certain time. Linear regression was used to determine the relationship between component-dominance and behavior over time.

To determine total extent of session discriminability of TCA-identified components, pooled TCA models were generated 100 times for each group and compared to models generated on 100 shuffled datasets from the same groups using unpaired t-tests. Neurons were randomly shuffled at each timepoint so as to preserve the within- and across-trial temporal structure of the data, controlling for changes in recording quality across days. To compare across groups, neurons were randomly subsampled in each iteration of TCA to control for effects of the number of cells on session discriminability.

As TCA also assigns weights to each neuron in each component, we found we could use this information to identify ensembles of neurons driving each component.

Identifying neural ensembles: TCA returns neuron factor loadings signifying the relative weight of each neuron in a given component. However, the absolute values of these weights are influenced by the size of the data tensor across all three dimensions. To determine the neuron factor loading or weight above which a neuron would be contributing to a component greater than by chance, simulated data tensors were generated for each animal populated with identically behaving neurons. For animal *a* with *c* longitudinally recorded neurons, given a constant experimental structure of T = 34 total trials with t = 60 sec per trial, a tensor of 60 sec x c_a x 34 trials was generated and TCA iterated 100x. We chose a threshold of w=1.0 as the median and mean of the null distribution of the factor loading threshold were greater than 1.0 and less than 1.1. Primary outcomes (See **Fig. 5B-D, Supp. Fig. 6**) were re-calculated using various factor thresholds to verify that results with a threshold w=1.0 are robust to threshold choice. Thus, *Acq*-dominant ensemble, for instance, was therefore comprised of neurons with w>1 in the *Acq*-dominant component determined by the strength metric described above.

Fisher linear discriminant analysis: A Fisher decoder was trained in Matlab on one of seven predictors: the mean activity of the *Acq-Only, Ext1-Only, Ext3-Only, Acq/Ext1, Acq/Ext3, Ext1/Ext3*, or *Acq/Ext1/Ext3* ensembles over all timepoints in a given session. Class labels were "Responders," "Non-responders," or "Saline" mice. Fisher decoders were trained to distinguish between data from two of the class labels in order to determine how similar or different the ensembles between particular pairs of groups behaved. Fisher decoders were trained on a randomly selected 50% of the data and tested on the other 50% over 100 iterations. As a control, class labels were randomly shuffled and model performance was tested on the shuffled data. If the accuracies of the decoders generated by a given ensemble's activity overlapped with the distribution of accuracies when tested on shuffled data, it was classified as failing to predict responder status or treatment. If not, then this ensemble was classified as predictive with respect to the given distinction.

Acknowledgements.

This work was supported by NIH NIGMS DP2GM140923 awarded to G.C. We thank the University Laboratory Animal Resources (ULAR) group at the University of Pennsylvania for assistance with rodent husbandry and veterinary support, including all faculty stationed at both the Translational Research Laboratory. Thanks to Stephen Wisser (Penn) for assistance running behavioral experiments in Figure 1. We would also like to thank other members of the Corder Lab, Adrienne Jo (Penn) and Raquel Adaia Sandoval Ortega (Penn) for critical discussions and advice on behavioral analysis, data visualization, and analysis validation. We would also like to thank Colin Mackey for assistance in customizing python packages. Finally, we would like to thank the faculty of the Cold Spring Harbor Laboratory course in Neural Data Analysis for critical input on analysis approach.

Author contributions.

S.R. and G.C. conceptualized and planned the study. E.H. provided key resources including psilocybin and assisted with experimental design and behavioral analysis. S.R. performed all data collection, analysis, and writing. G.C. acquired funding, performed data visualization along with S.R., and edited and revised manuscript.

Declaration of competing interests.

The authors declare no competing interests.

References.

1. Hoppen, Thole H, Stefan Priebe, Inja Vetter, and Nexhmedin Morina. "Global Burden of Post-Traumatic Stress Disorder and Major Depression in Countries Affected by War between 1989 and 2019: A Systematic Review and Meta-Analysis." *BMJ Global Health* 6, no. 7 (July 2021): e006303. https://doi.org/10.1136/bmjgh-2021-006303.

2. Nutt, David, and Robin Carhart-Harris. "The Current Status of Psychedelics in Psychiatry." *JAMA Psychiatry* 78, no. 2 (February 1, 2021): 121–22. https://doi.org/10.1001/jamapsychiatry.2020.2171.
3. Griffiths, R. R., M.W. Johnson, W. A. Richards, B.D. Richards, U. McCann, and R. Jesse. "Psilocybin Occasioned Mystical-Type Experiences: Immediate and Persisting Dose-Related Effects." *Psychopharmacology* 218, no. 4 (December 2011): 649–65. https://doi.org/10.1007/s00213-011-2358-5.
4. Agin-Liebes, Gabrielle I, Tara Malone, Matthew M Yalch, Sarah E Mennenga, K Linnae Ponté, Jeffrey Guss, Anthony P Bossis, Jim Grigsby, Stacy Fischer, and Stephen Ross. "Long-Term Follow-up of Psilocybin-Assisted Psychotherapy for Psychiatric and Existential Distress in Patients with Life-Threatening Cancer." *Journal of Psychopharmacology* 34, no. 2 (February 1, 2020): 155–66. https://doi.org/10.1177/0269881119897615.
5. Aday, Jacob S., Cayla M. Mitzkovitz, Emily K. Bloesch, Christopher C. Davoli, and Alan K. Davis. "Long-Term Effects of Psychedelic Drugs: A Systematic Review." *Neuroscience & Biobehavioral Reviews* 113 (June 1, 2020): 179–89. https://doi.org/10.1016/j.neubiorev.2020.03.017.
6. Gukasyan, Natalie, Alan K Davis, Frederick S Barrett, Mary P Cosimano, Nathan D Sepeda, Matthew W Johnson, and Roland R Griffiths. "Efficacy and Safety of Psilocybin-Assisted Treatment for Major Depressive Disorder: Prospective 12-Month Follow-Up." *Journal of Psychopharmacology* 36, no. 2 (February 1, 2022): 151–58. https://doi.org/10.1177/02698811211073759.
7. Hesselgrave, Natalie, Timothy A. Troppoli, Andreas B. Wulff, Anthony B. Cole, and Scott M. Thompson. "Harnessing Psilocybin: Antidepressant-like Behavioral and Synaptic Actions of Psilocybin Are Independent of 5-HT2R Activation in Mice." *Proceedings of the National Academy of Sciences of the United States of America* 118, no. 17 (April 27, 2021): e2022489118. https://doi.org/10.1073/pnas.2022489118.
8. Cameron, Lindsay P., Seona D. Patel, Maxemiliano V. Vargas, Eden V. Barragan, Hannah N. Saeger, Hunter T. Warren, Winston L. Chow, John A. Gray, and David E. Olson. "5-HT2ARs Mediate Therapeutic Behavioral Effects of Psychedelic Tryptamines." *ACS Chemical Neuroscience* 14, no. 3 (February 1, 2023): 351–58. https://doi.org/10.1021/acschemneuro.2c00718.
9. Hibicke, Meghan, Hannah M. Kramer, and Charles D. Nichols. "A Single Administration of Psilocybin Persistently Rescues Cognitive Deficits Caused by Adolescent Chronic Restraint Stress Without Long-Term Changes in Synaptic Protein Gene Expression in a Rat Experimental System with Translational Relevance to Depression." *Psychedelic Medicine*, March 3, 2023. https://doi.org/10.1089/psymed.2022.0012.
10. Hernandez-Leon, Alberto, Raúl Iván Escamilla-Orozco, Aylín R. Tabal-Robles, David Martínez-Vargas, Leticia Romero-Bautista, Gerson Escamilla-Soto, Osiris S. González-Romero, Martín Torres-Valencia, and María Eva González-Trujano. "Antidepressant- and Anxiolytic-like Activities and Acute Toxicity Evaluation of the Psilocybe Cubensis Mushroom in Experimental Models in Mice." *Journal of Ethnopharmacology* 320 (February 10, 2024): 117415. https://doi.org/10.1016/j.jep.2023.117415.
11. Jones, Nathan T, Zarmeen Zahid, Sean M Grady, Ziyad W Sultan, Zhen Zheng, Matthew I Banks, and Cody J Wenthur. "Delayed Anxiolytic-Like Effects of Psilocybin in Male Mice Are Supported by Acute Glucocorticoid Release." Preprint. Animal Behavior and Cognition, August 14, 2020. https://doi.org/10.1101/2020.08.12.248229.
12. Jones, Nathan T., Zarmeen Zahid, Sean M. Grady, Ziyad W. Sultan, Zhen Zheng, John Razidlo, Matthew I. Banks, and Cody J. Wenthur. "Transient Elevation of Plasma Glucocorticoids Supports Psilocybin-Induced Anxiolysis in Mice." *ACS Pharmacology & Translational Science* 6, no. 8 (August 11, 2023): 1221–31. https://doi.org/10.1021/acsptsci.3c00123.
13. Takaba, Rika, Daisuke Ibi, Keisuke Yoshida, Eri Hosomi, Ririna Kawase, Hiroko Kitagawa, Hirotaka Goto, et al. "Ethopharmacological Evaluation of Antidepressant-like Effect of Serotonergic Psychedelics in C57BL/6J Male Mice." *Naunyn-Schmiedeberg's Archives of Pharmacology*, October 24, 2023. https://doi.org/10.1007/s00210-023-02778-x.
14. Odland, Anna U., Jesper L. Kristensen, and Jesper T. Andreasen. "Investigating the Role of 5-HT2A and 5-HT2C Receptor Activation in the Effects of Psilocybin, DOI, and Citalopram on Marble Burying in Mice." *Behavioural Brain Research* 401 (March 5, 2021): 113093. https://doi.org/10.1016/j.bbr.2020.113093.
15. Wulff, Andreas B., Charles D. Nichols, and Scott M. Thompson. "Preclinical Perspectives on the Mechanisms Underlying the Therapeutic Actions of Psilocybin in Psychiatric Disorders." *Neuropharmacology* 231 (June 15, 2023): 109504. https://doi.org/10.1016/j.neuropharm.2023.109504.
16. Passie, Torsten, Juergen Seifert, Udo Schneider, and Hinderk M. Emrich. "The Pharmacology of Psilocybin." *Addiction Biology* 7, no. 4 (2002): 357–64. https://doi.org/10.1080/1355621021000005937.
17. Lowe, Henry, Ngeh Toyang, Blair Steele, Henkel Valentine, Justin Grant, Amza Ali, Wilfred Ngwa, and Lorenzo Gordon. "The Therapeutic Potential of Psilocybin." *Molecules (Basel, Switzerland)* 26, no. 10 (May 15, 2021): 2948. https://doi.org/10.3390/molecules26102948.
18. Garcia-Romeu, Albert, Roland R. Griffiths, and Matthew W. Johnson. "Psilocybin-Occasioned Mystical Experiences in the Treatment of Tobacco Addiction." *Current Drug Abuse Reviews* 7, no. 3 (2015): 157–64.
19. Bremler, Rebecka, Nancy Katati, Parvinder Shergill, David Erritzoe, and Robin L. Carhart-Harris. "Case Analysis of Long-Term Negative Psychological Responses to Psychedelics." *Scientific Reports* 13 (September 25, 2023): 15998. https://doi.org/10.1038/s41598-023-41145-x.
20. Simonsson, Otto, Per Carlbring, Robin Carhart-Harris, Alan K. Davis, David J. Nutt, Roland R. Griffiths, David Erritzoe, and Simon B. Goldberg. "Assessing the Risk of Symptom Worsening in Psilocybin-Assisted Therapy for Depression: A Systematic Review and Individual Participant Data Meta-Analysis." *Psychiatry Research* 327 (September 1, 2023): 115349. https://doi.org/10.1016/j.psychres.2023.115349.
21. Simonsson, Otto, Peter S. Hendricks, Richard Chambers, Walter Osika, and Simon B. Goldberg. "Prevalence and Associations of Challenging, Difficult or Distressing Experiences Using Classic Psychedelics." *Journal of Affective Disorders* 326 (April 1, 2023): 105–10. https://doi.org/10.1016/j.jad.2023.01.073.
22. Breeksema, Joost J, Bouwe W Kuin, Jeanine Kamphuis, Wim van den Brink, Eric Vermetten, and Robert A Schoevers. "Adverse Events in Clinical Treatments with Serotonergic Psychedelics and MDMA: A Mixed-Methods

Systematic Review." *Journal of Psychopharmacology (Oxford, England)* 36, no. 10 (October 2022): 1100–1117. https://doi.org/10.1177/02698811221116926.
23. Lewis, Candace R., Katrin H. Preller, B. Blair Braden, Cory Riecken, and Franz X. Vollenweider. "Rostral Anterior Cingulate Thickness Predicts the Emotional Psilocybin Experience." *Biomedicines* 8, no. 2 (February 18, 2020):
24. Halim, Haniya J., Bradley G. Burk, Rachel E. Fargason, and Badari Birur. "Manic Episode Following Psilocybin Use in a Man with Bipolar II Disorder: A Case Report." *Frontiers in Psychiatry* 14 (2023): 1221131. https://doi.org/10.3389/fpsyt.2023.1221131.
25. Borkel, Lucas F., Jaime Rojas-Hernández, Luis Alberto Henríquez-Hernández, Ángelo Santana Del Pino, and Domingo J. Quintana-Hernández. "Set and Setting Predict Psychopathology, Wellbeing and Meaningfulness of Psychedelic Experiences: A Correlational Study." *Expert Review of Clinical Pharmacology*, December 18, 2023. https://doi.org/10.1080/17512433.2023.2295997.
26. Kettner, Hannes, Sam Gandy, Eline C. H. M. Haijen, and Robin L. Carhart-Harris. "From Egoism to Ecoism: Psychedelics Increase Nature Relatedness in a State-Mediated and Context-Dependent Manner." *International Journal of Environmental Research and Public Health* 16, no. 24 (December 16, 2019): 5147. https://doi.org/10.3390/ijerph16245147.
27. Faillace, L. A., and S. Szara. "Hallucinogenic Drugs: Influence of Mental Set and Setting." *Diseases of the Nervous System* 29, no. 2 (February 1968): 124–26.
28. Heinzerling, Keith G., Karina Sergi, Micah Linton, Rhianna Rich, Brittany Youssef, Inez Bentancourt, Jennifer Bramen, Prabha Siddarth, Louie Schwartzberg, and Daniel F. Kelly. "Nature-Themed Video Intervention May Improve Cardiovascular Safety of Psilocybin-Assisted Therapy for Alcohol Use Disorder." *Frontiers in Psychiatry* 14 (September 18, 2023): 1215972. https://doi.org/10.3389/fpsyt.2023.1215972.
29. Haijen, Eline C. H. M., Mendel Kaelen, Leor Roseman, Christopher Timmermann, Hannes Kettner, Suzanne Russ, David Nutt, et al. "Predicting Responses to Psychedelics: A Prospective Study." *Frontiers in Pharmacology* 9 (November 2, 2018): 897. https://doi.org/10.3389/fphar.2018.00897.
30. Strickland, JustinC., Albert Garcia-Romeu, and Matthew W. Johnson. "Set and Setting: A Randomized Study of Different Musical Genres in Supporting Psychedelic Therapy." *ACS Pharmacology & Translational Science* 4, no. 2 (December 29, 2020): 472–78. https://doi.org/10.1021/acsptsci.0c00187.
31. Davis, Alan K., Frederick S. Barrett, and Roland R. Griffiths. "Psychological Flexibility Mediates the Relations between Acute Psychedelic Effects and Subjective Decreases in Depression and Anxiety." *Journal of Contextual Behavioral Science* 15 (January 2020): 39–45. https://doi.org/10.1016/j.jcbs.2019.11.004.
32. Doss, Manoj K., Michal Považan, Monica D. Rosenberg, Nathan D. Sepeda, Alan K. Davis, Patrick H. Finan, Gwenn S. Smith, et al. "Psilocybin Therapy Increases Cognitive and Neural Flexibility in Patients with Major Depressive Disorder." *Translational Psychiatry* 11, no. 1 (November 8, 2021): 574. https://doi.org/10.1038/s41398-021-01706-y.
33. Pacheco, Alejandro Torrado, Randall J. Olson, Gabriela Garza, and Bita Moghaddam. "Acute Psilocybin Enhances Cognitive Flexibility in Rats." bioRxiv, January 9, 2023. https://doi.org/10.1101/2023.01.09.523291.
34. Conn, K., L. K. Milton, K. Huang, H. Munguba, J. Ruuska, M. B. Lemus, E. Greaves, J. Homman-Ludiye, B. J. Oldfield, and C. J. Foldi. "Psilocybin Prevents Activity-Based Anorexia in Female Rats by Enhancing Cognitive Flexibility: Contributions from 5-HT1A and 5-HT2A Receptor Mechanisms." bioRxiv, December 13, 2023. https://doi.org/10.1101/2023.12.12.571374.
35. Price, Rebecca B., and Ronald Duman. "Neuroplasticity in Cognitive and Psychological Mechanisms of Depression: An Integrative Model." *Molecular Psychiatry* 25, no. 3 (March 2020): 530–43. https://doi.org/10.1038/s41380-019-0615-x.
36. Zhukovsky, Peter, Johan Alsiö, Bianca Jupp, Jing Xia, Chiara Guiliano, Lucy Jenner, Jessica Griffiths, et al. "Perseveration in a Spatial-Discrimination Serial Reversal Learning Task Is Differentially Affected by MAO-A and MAO-B Inhibition and Associated with Reduced Anxiety and Peripheral Serotonin Levels." *Psychopharmacology* 234, no. 9 (2017): 1557–71. https://doi.org/10.1007/s00213-017-4569-x.
37. Vargas, Maxemiliano V., Lee E. Dunlap, Chunyang Dong, Samuel J. Carter, Robert J. Tombari, Shekib A. Jami, Lindsay P. Cameron, et al. "Psychedelics Promote Neuroplasticity through the Activation of Intracellular 5-HT2A Receptors." *Science* 379, no. 6633 (February 17, 2023): 700–706. https://doi.org/10.1126/science.adf0435.
38. Carhart-Harris, R. L., and K. J. Friston. "REBUS and the Anarchic Brain: Toward a Unified Model of the Brain Action of Psychedelics." Edited by Eric L. Barker. *Pharmacological Reviews* 71, no. 3 (July 2019): 316–44. https://doi.org/10.1124/pr.118.017160.
39. Alonso, Joan Francesc, Sergio Romero, Miquel Àngel Mañanas, and Jordi Riba. "Serotonergic Psychedelics Temporarily Modify Information Transfer in Humans." *International Journal of Neuropsychopharmacology* 18, no. 8 (June 2015). https://doi.org/10.1093/ijnp/pyv039.
40. Ly, Calvin, Alexandra C. Greb, Lindsay P. Cameron, Jonathan M. Wong, Eden V. Barragan, Paige C. Wilson, Kyle F. Burbach, et al. "Psychedelics Promote Structural and Functional Neural Plasticity." *Cell Reports* 23, no. 11 (June 12, 2018): 3170–82. https://doi.org/10.1016/j.celrep.2018.05.022.
41. Olson, David E. "Psychoplastogens: A Promising Class of Plasticity-Promoting Neurotherapeutics." *Journal of Experimental Neuroscience* 12 (January 1, 2018): 1179069518800508. https://doi.org/10.1177/1179069518800508.
42. Shao, Ling-Xiao, Clara Liao, Ian Gregg, Pasha A. Davoudian, Neil K. Savalia, Kristina Delagarza, and Alex C. Kwan. "Psilocybin Induces Rapid and Persistent Growth of Dendritic Spines in Frontal Cortex in Vivo." *Neuron* 109, no. 16 (August 18, 2021): 2535-2544.e4. https://doi.org/10.1016/j.neuron.2021.06.008.
43. Ly, Calvin, Alexandra C. Greb, Maxemiliano V. Vargas, Whitney C. Duim, Ana Cristina G. Grodzki, Pamela J. Lein, and David E. Olson. "Transient Stimulation with Psychoplastogens Is Sufficient to Initiate Neuronal Growth." *ACS Pharmacology & Translational Science* 4, no. 2 (April 9, 2021): 452–60. https://doi.org/10.1021/acsptsci.0c00065.
44. Du, Yingjie, Yunfeng Li, Xiangting Zhao, Yishan Yao, Bin Wang, Liming Zhang, and Guyan Wang. "Psilocybin Facilitates Fear Extinction in Mice by Promoting Hippocampal Neuroplasticity." *Chinese Medical Journal*, March 30, 2023. https://doi.org/10.1097/CM9.0000000000002647.

45. Moliner, Rafael, Mykhailo Girych, Cecilia A. Brunello, Vera Kovaleva, Caroline Biojone, Giray Enkavi, Lina Antenucci, et al. "Psychedelics Promote Plasticity by Directly Binding to BDNF Receptor TrkB." *Nature Neuroscience* 26, no. 6 (June 2023): 1032–41. https://doi.org/10.1038/s41593-023-01316-5.
46. Schmitz, Gavin P., Yi-Ting Chiu, Gabriele M. König, Evi Kostenis, Bryan L. Roth, and Melissa A. Herman. "Psychedelic Compounds Directly Excite 5-HT2A Layer 5 Pyramidal Neurons in the Prefrontal Cortex through a 5-HT2A Gq -Mediated Activation Mechanism." bioRxiv, November 15, 2022. https://doi.org/10.1101/2022.11.15.516655.
47. Vann, Seralynne D., John P. Aggleton, and Eleanor A. Maguire. "What Does the Retrosplenial Cortex Do?" *Nature Reviews Neuroscience* 10, no. 11 (November 2009): 792–802. https://doi.org/10.1038/nrn2733.
48. Summerfield, Jennifer J., Demis Hassabis, and Eleanor A. Maguire. "Cortical Midline Involvement in Autobiographical Memory." *Neuroimage* 44, no. 3 (February 1, 2009): 1188–1200. https://doi.org/10.1016/j.neuroimage.2008.09.033.
49. Maguire, E A. "Neuroimaging Studies of Autobiographical Event Memory." *Philosophical Transactions of the Royal Society of London. Series B* 356, no. 1413 (September 29, 2001): 1441–51. https://doi.org/10.1098/rstb.2001.0944.
50. Todd, Travis P., Nicole E. DeAngeli, Matthew Y. Jiang, and David J. Bucci. "Retrograde Amnesia of Contextual Fear Conditioning: Evidence for Retrosplenial Cortex Involvement in Configural Processing." *Behavioral Neuroscience* 135 (2021): 453–61. https://doi.org/10.1037/bne0000432.
51. Todd, Travis P., and David J. Bucci. "Retrosplenial Cortex and Long-Term Memory: Molecules to Behavior." *Neural Plasticity* 2015 (2015): 414173. https://doi.org/10.1155/2015/414173.
52. Miller, Adam M P, Anna C Serrichio, and David M Smith. "Dual-Factor Representation of the Environmental Context in the Retrosplenial Cortex." *Cerebral Cortex* 31, no. 5 (May 1, 2021): 2720–28. https://doi.org/10.1093/cercor/bhaa386.
53. Hattori, Ryoma, and Takaki Komiyama. "Context-Dependent Persistency as a Coding Mechanism for Robust and Widely Distributed Value Coding." *Neuron* 110, no. 3 (February 2022): 502-515.e11. https://doi.org/10.1016/j.neuron.2021.11.001.
54. Sun, Weilun, Ilseob Choi, Stoyan Stoyanov, Oleg Senkov, Evgeni Ponimaskin, York Winter, Janelle M. P. Pakan, and Alexander Dityatev. "Context Value Updating and Multidimensional Neuronal Encoding in the Retrosplenial Cortex." *Nature Communications* 12, no. 1 (October 18, 2021): 6045. https://doi.org/10.1038/s41467-021-26301-z.
55. Trask, Sydney, Nicole C. Ferrara, Aaron M. Jasnow, and Janine L. Kwapis. "Contributions of the Rodent Cingulate-Retrosplenial Cortical Axis to Associative Learning and Memory: A Proposed Circuit for Persistent Memory Maintenance." *Neuroscience & Biobehavioral Reviews* 130 (November 2021): 178–84. https://doi.org/10.1016/j.neubiorev.2021.08.023.
56. Trask, Sydney, and Fred J Helmstetter. "Unique Roles for the Anterior and Posterior Retrosplenial Cortices in Encoding and Retrieval of Memory for Context." *Cerebral Cortex* 32, no. 17 (August 22, 2022): 3602–10. https://doi.org/10.1093/cercor/bhab436.
57. Mitchell, Anna S., Rafal Czajkowski, Ningyu Zhang, Kate Jeffery, and Andrew J. D. Nelson. "Retrosplenial Cortex and Its Role in Spatial Cognition." *Brain and Neuroscience Advances* 2 (2018): 2398212818757098. https://doi.org/10.1177/2398212818757098.
58. Brennan, Ellen KW, Izabela Jedrasiak-Cape, Sameer Kailasa, Sharena P Rice, Shyam Kumar Sudhakar, and Omar J Ahmed. "Thalamus and Claustrum Control Parallel Layer 1 Circuits in Retrosplenial Cortex." *eLife* 10 (June 25, 2021): e62207. https://doi.org/10.7554/eLife.62207.
59. Cheng, Ning, Qiqi Dong, Zhen Zhang, Li Wang, Xiaojing Chen, and Cheng Wang. "Egocentric Processing of Items in Spines, Dendrites, and Somas in the Retrosplenial Cortex." *Neuron* 0, no. 0 (December 14, 2023). https://doi.org/10.1016/j.neuron.2023.11.018.
60. Carhart-Harris, Robin L., Suresh Muthukumaraswamy, Leor Roseman, Mendel Kaelen, Wouter Droog, Kevin Murphy, Enzo Tagliazucchi, et al. "Neural Correlates of the LSD Experience Revealed by Multimodal Neuroimaging." *Proceedings of the National Academy of Sciences* 113, no. 17 (April 26, 2016): 4853–58. https://doi.org/10.1073/pnas.1518377113.
61. Wang, Guangyu, Hong Xie, Lun Wang, Wenhan Luo, Yixiang Wang, Jun Jiang, Chun Xiao, Feng Xing, and Ji-Song Guan. "Switching From Fear to No Fear by Different Neural Ensembles in Mouse Retrosplenial Cortex." *Cerebral Cortex* 29, no. 12 (December 17, 2019): 5085–97. https://doi.org/10.1093/cercor/bhz050.
62. Zhang, Kai, Dan Shen, Shihao Huang, Javed Iqbal, Gengdi Huang, Jijian Si, Yanxue Xue, and Jian-Li Yang. "The Sexually Divergent cFos Activation Map of Fear Extinction." *Heliyon* 10, no. 1 (January 15, 2024): e23748. https://doi.org/10.1016/j.heliyon.2023.e23748.
63. Davoudian, Pasha A., Ling-Xiao Shao, and Alex C. Kwan. "Shared and Distinct Brain Regions Targeted for Immediate Early Gene Expression by Ketamine and Psilocybin." *ACS Chemical Neuroscience* 14, no. 3 (February 1, 2023): 468–80. https://doi.org/10.1021/acschemneuro.2c00637.
64. Kometer, Michael, André Schmidt, Lutz Jäncke, and Franz X. Vollenweider. "Activation of Serotonin 2A Receptors Underlies the Psilocybin-Induced Effects on α Oscillations, N170 Visual-Evoked Potentials, and Visual Hallucinations." *Journal of Neuroscience* 33, no. 25 (June 19, 2013): 10544–51. https://doi.org/10.1523/JNEUROSCI.3007-12.2013.
65. Liu, Shijing, Marcy J. Bubar, Maria Fe Lanfranco, Gilbert R. Hillman, and Kathryn A. Cunningham. "Serotonin2C Receptor (5-HT2CR) Localization in GABA Neurons of the Rat Medial Prefrontal Cortex: Implications for Understanding the Neurobiology of Addiction." *Neuroscience* 146, no. 4 (June 8, 2007): 1677–88. https://doi.org/10.1016/j.neuroscience.2007.02.064.
66. Pompeiano, M., J. M. Palacios, and G. Mengod. "Distribution of the Serotonin 5-HT2 Receptor Family mRNAs: Comparison between 5-HT2A and 5-HT2C Receptors." *Molecular Brain Research* 23, no. 1 (April 1, 1994): 163–78. https://doi.org/10.1016/0169-328X(94)90223-2.
67. Zhang, Yajuan, Chu-Chung Huang, Jiajia Zhao, Yuchen Liu, Mingrui Xia, Xiaoqin Wang, Dongtao Wei, et al. "Resting-State Functional Connectivity of the Raphe Nuclei in Major Depressive Disorder: A Multi-Site Study." *NeuroImage: Clinical* 37 (February 24, 2023): 103359. https://doi.org/10.1016/j.nicl.2023.103359.
68. Corcoran, Kevin A., Michael D. Donnan, Natalie C. Tronson, Yomayra F. Guzmán, Can Gao, Vladimir Jovasevic, Anita

L. Guedea, and Jelena Radulovic. "NMDA Receptors in Retrosplenial Cortex Are Necessary for Retrieval of Recent and Remote Context Fear Memory." *The Journal of Neuroscience* 31, no. 32 (August 10, 2011): 11655–59. https://doi.org/10.1523/JNEUROSCI.2107-11.2011.

69. Corcoran, Kevin A., Brendan J. Frick, Jelena Radulovic, and Leslie M. Kay. "Analysis of Coherent Activity between Retrosplenial Cortex, Hippocampus, Thalamus, and Anterior Cingulate Cortex during Retrieval of Recent and Remote Context Fear Memory." *Neurobiology of Learning and Memory* 127 (January 2016): 93–101. https://doi.org/10.1016/j.nlm.2015.11.019.
70. Auguste, Anne, Nicolas Fourcaud-Trocmé, David Meunier, Alexandra Gros, Samuel Garcia, Belkacem Messaoudi, Marc Thevenet, Nadine Ravel, and Alexandra Veyrac. "Distinct Brain Networks for Remote Episodic Memory Depending on Content and Emotional Value." bioRxiv, September 19, 2022. https://doi.org/10.1101/2022.09.16.508241.
71. Todd, Travis P., Max L. Mehlman, Christopher S. Keene, Nicole E. DeAngeli, and David J. Bucci. "Retrosplenial Cortex Is Required for the Retrieval of Remote Memory for Auditory Cues." *Learning & Memory* 23, no. 6 (June 2016): 278–88. https://doi.org/10.1101/lm.041822.116.
72. Fournier, Danielle I., Han Yin Cheng, Armin Tavakkoli, Allan T. Gulledge, David J. Bucci, and Travis P. Todd. "Retrosplenial Cortex Inactivation during Retrieval, but Not Encoding, Impairs Remotely Acquired Auditory Fear Conditioning in Male Rats." *Neurobiology of Learning and Memory* 185 (November 2021): 107517. https://doi.org/10.1016/j.nlm.2021.107517.
73. Kwapis, Janine L., Timothy J. Jarome, Jonathan L. Lee, Marieke R. Gilmartin, and Fred J. Helmstetter. "Extinguishing Trace Fear Engages the Retrosplenial Cortex Rather than the Amygdala." *Neurobiology of Learning and Memory* 113 (September 2014): 41–54. https://doi.org/10.1016/j.nlm.2013.09.007.
74. Trask, Sydney, Nicole C. Ferrara, Kevin Grisales, and Fred J. Helmstetter. "Optogenetic Inhibition of Either the Anterior or Posterior Retrosplenial Cortex Disrupts Retrieval of a Trace, but Not Delay, Fear Memory." *Neurobiology of Learning and Memory* 185 (November 2021): 107530. https://doi.org/10.1016/j.nlm.2021.107530.
75. Han, C. J., Colm M. O'Tuathaigh, Laurent van Trigt, Jennifer J. Quinn, Michael S. Fanselow, Raymond Mongeau, Christof Koch, and David J. Anderson. "Trace but Not Delay Fear Conditioning Requires Attention and the Anterior Cingulate Cortex." *Proceedings of the National Academy of Sciences of the United States of America* 100, no. 22 (October 28, 2003): 13087–92. https://doi.org/10.1073/pnas.2132313100.
76. Cowansage, Kiriana Kater, Tristan Shuman, Blythe Christine Dillingham, Allene Chang, Peyman Golshani, and Mark Mayford. "Direct Reactivation of a Coherent Neocortical Memory of Context." *Neuron* 84, no. 2 (October 22, 2014): 432–41. https://doi.org/10.1016/j.neuron.2014.09.022.
77. Catlow, Briony J., Shijie Song, Daniel A. Paredes, Cheryl L. Kirstein, and Juan Sanchez-Ramos. "Effects of Psilocybin on Hippocampal Neurogenesis and Extinction of Trace Fear Conditioning." *Experimental Brain Research* 228, no. 4 (August 1, 2013): 481–91. https://doi.org/10.1007/s00221-013-3579-0.
78. Williams, Alex H., Tony Hyun Kim, Forea Wang, Saurabh Vyas, Stephen I. Ryu, Krishna V. Shenoy, Mark Schnitzer, Tamara G. Kolda, and Surya Ganguli. "Unsupervised Discovery of Demixed, Low-Dimensional Neural Dynamics across Multiple Timescales through Tensor Component Analysis." *Neuron* 98, no. 6 (June 27, 2018): 1099-1115.e8. https://doi.org/10.1016/j.neuron.2018.05.015.
79. Pennington, Zachary T., Zhe Dong, Yu Feng, Lauren M. Vetere, Lucia Page-Harley, Tristan Shuman, and Denise J. Cai. "ezTrack: An Open-Source Video Analysis Pipeline for the Investigation of Animal Behavior." *Scientific Reports* 9, no. 1 (December 27, 2019): 19979. https://doi.org/10.1038/s41598-019-56408-9.
80. Wyrick, David G, Nicholas Cain, Rylan S. Larsen, Jérôme Lecoq, Matthew Valley, Ruweida Ahmed, Jessica Bowlus, et al. "Differential Encoding of Temporal Context and Expectation under Representational Drift across Hierarchically Connected Areas." *bioRxiv*, June 5, 2023, 2023.06.02.543483. https://doi.org/10.1101/2023.06.02.543483.
81. Ekins, Tyler G, Isla Brooks, Sameer Kailasa, Chloe Rybicki-Kler, Izabela Jedrasiak-Cape, Ethan Donoho, George A. Mashour, Jason Rech, and Omar J Ahmed. "Cellular Rules Underlying Psychedelic Control of Prefrontal Pyramidal Neurons." Preprint. Neuroscience, October 23, 2023. https://doi.org/10.1101/2023.10.20.563334.
82. Tomé, Douglas Feitosa, Ying Zhang, Tomomi Aida, Olivia Mosto, Yifeng Lu, Mandy Chen, Sadra Sadeh, Dheeraj S. Roy, and Claudia Clopath. "Dynamic and Selective Engrams Emerge with Memory Consolidation." *Nature Neuroscience*, January 19, 2024, 1–12. https://doi.org/10.1038/s41593-023-01551-w.
83. Effinger, D. P., S. G. Quadir, M. C. Ramage, M. G. Cone, and M. A. Herman. "Sex-Specific Effects of Psychedelic Drug Exposure on Central Amygdala Reactivity and Behavioral Responding." *Translational Psychiatry* 13, no. 1 (April 8, 2023): 119. https://doi.org/10.1038/s41398-023-02414-5.
84. Kwan, Alex C., David E. Olson, Katrin H. Preller, and Bryan L. Roth. "The Neural Basis of Psychedelic Action." *Nature Neuroscience* 25, no. 11 (November 2022): 1407–19. https://doi.org/10.1038/s41593-022-01177-4.

Supplementary Materials.

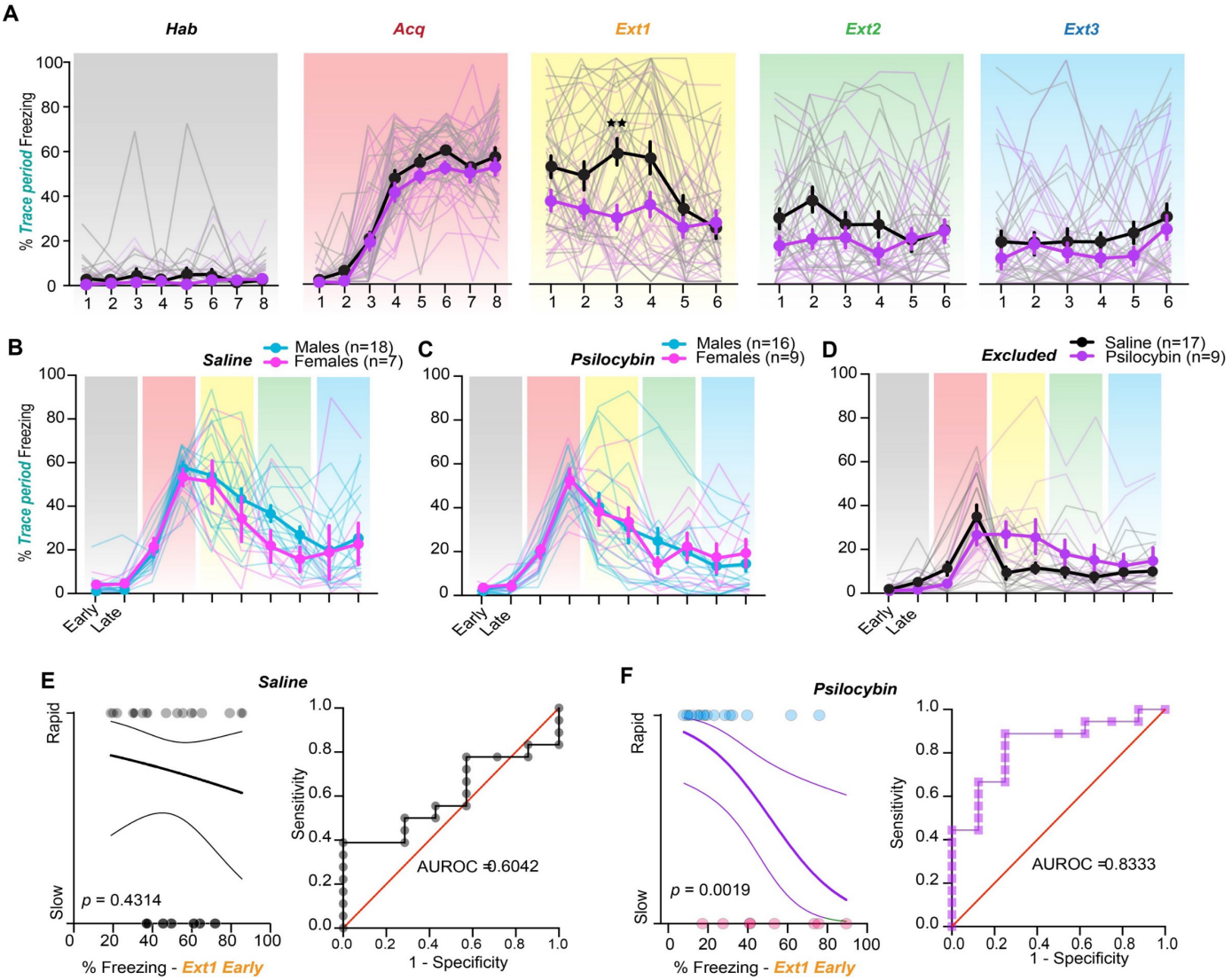

Supplementary Figure 1 | Effects of psilocybin on trace fear extinction in males and females.
(A) Trial by trial freezing of saline- and psilocybin-administered mice. Two-Way RM ANOVA with Sidak multiple comparisons correction. (Supp. Table 1, rows 66-70). **(B)** Half-session freezing by sex of saline-administered animals. Two-Way RM ANOVA with Sidak multiple comparisons correction. (Supp. Table 1, rows 71). **(C)** Half-session freezing by sex of psilocybin-administered animals. Two-Way RM ANOVA with Sidak multiple comparisons correction. (Supp. Table 1, rows 72). **(D)** *Left*: Logistic regression predicting RE or SE status based on % time freezing during the first half of *Extinction 1* during acute drug treatment in saline-administered mice. *Right*: ROC curve from logistic regression. (Supp. Table 1, rows 12-13). **(E)** *Left*: Logistic regression predicting RE or SE status based on % time freezing during the first half of *Extinction 1* during acute drug treatment in saline-administered mice. *Right*: ROC curve from logistic regression. (Supp. Table 1, rows 14-15). * $p \leq 0.05$, ** $p < 0.01$, *** $p < 0.001$, **** $p < 0.0001$

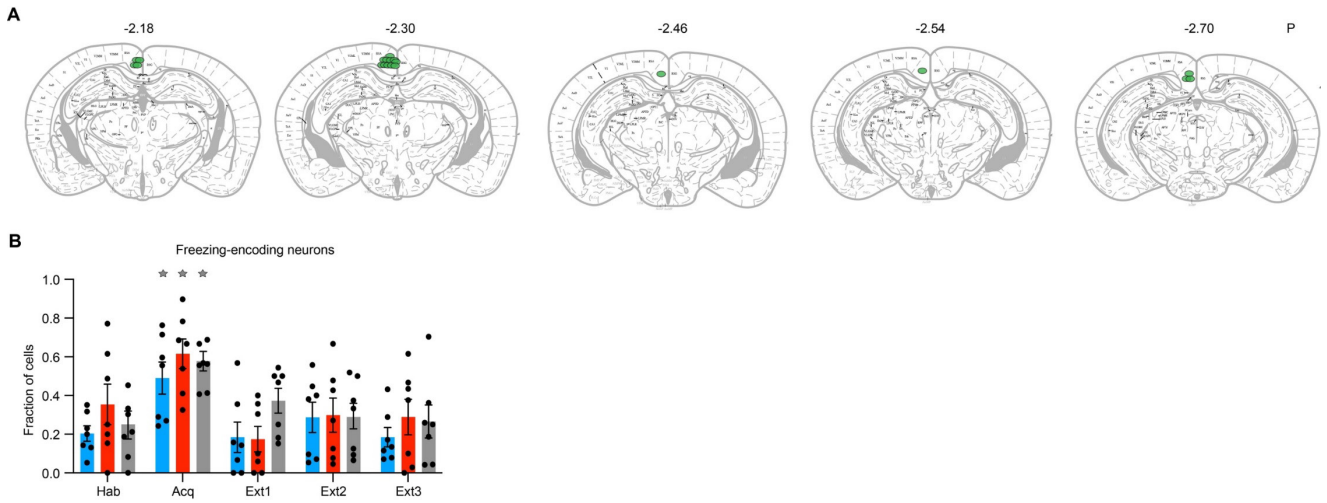

Supplementary Figure 2 | GRIN lens implant locations.
(A) Center and bottom of implant tracts of all included mice from anterior (left) to posterior (right) granular RSC. **(B)** Fraction of freezing encoding neurons on each day. Two-way RM ANOVA. (Supp. Table 1, rows 74). Data are represented as mean ± SEM. * $p \leq 0.05$, ** $p < 0.01$, *** $p < 0.001$, **** $p < 0.0001$

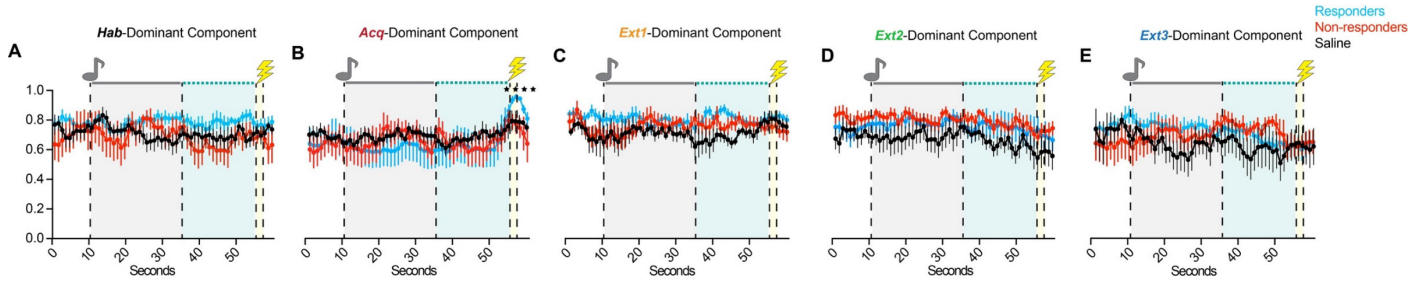

Supplementary Figure 3 | TCA factors reveal RSC dynamics modulated by session.
(A) Normalized temporal factor weights by group of the Habituation-dominant component. Two-Way RM ANOVA. (Supp. Table 1, rows 75). **(B)** Same as A) for the Acquisition-dominant component. Two-Way RM ANOVA. (Supp. Table 1, rows 76). **(C)** Same as A) for the Extinction 1-dominant component. Two-Way RM ANOVA. (Supp. Table 1, rows 77). **(D)** Same as A) for the Extinction 2-dominant component. Two-Way RM ANOVA. (Supp. Table 1, rows 78). **(E)** Same as A) for the Extinction 3-dominant component. (Supp. Table 1, rows 79). Data are represented as mean ± SEM. * $p \leq 0.05$, ** $p < 0.01$, *** $p < 0.001$, **** $p < 0.0001$.

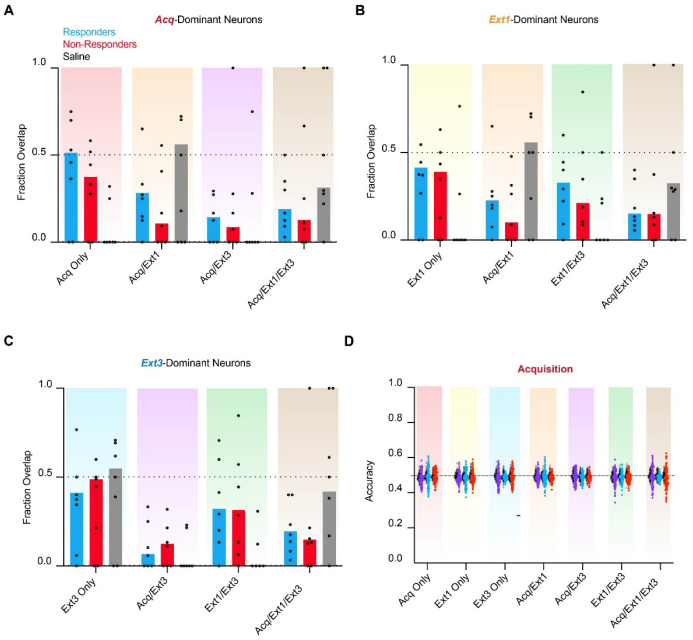

Supplementary Figure 4 | Psilocybin bidirectionally modulates neural ensembles driving RSC dynamics during TFC in responders.
(A) Overlaps of ensembles within individual animals comprising the mean values in Fig. 4B top. Bars are median. **(B)** Same as A) for Fig. 4B middle. **(C)** Same as A) for Fig. 4B middle. **(D)** Fisher decoder performance on Acquisition activity in functionally defined ensembles of cells to distinguish responders vs. non-responders (purple), responders vs. saline (blue around grey), and non-responders vs. saline (red around grey). 100 iterations for each comparison. Shuffled values are behind real values.

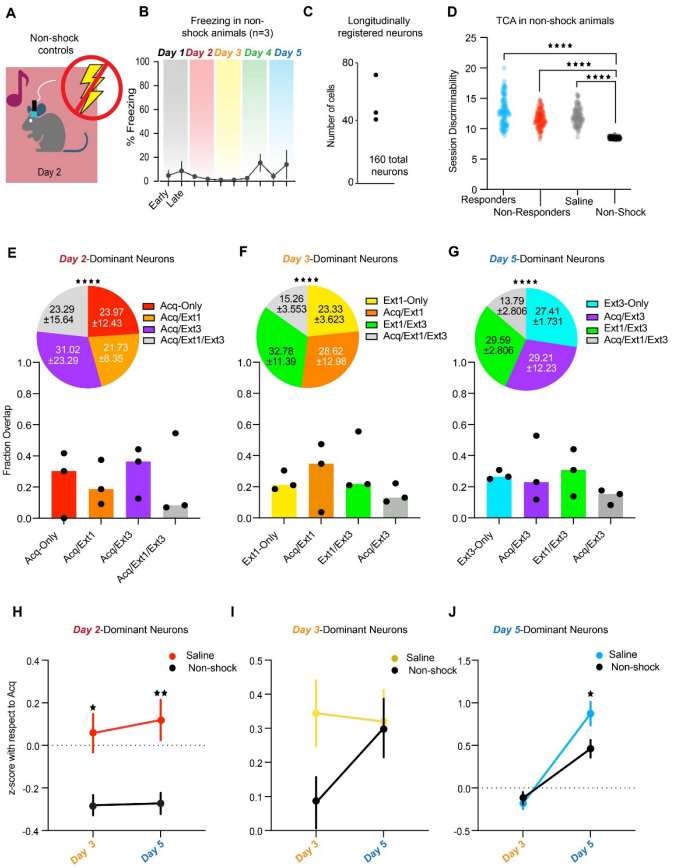

Supplementary Figure 5 | Non-shock controls do not exhibit conditioning-associated dynamics.
(A) Schematic of non-shock protocol. 3 miniscope implanted mice underwent identical 5 day paradigm to all other mice, with the exception that they received no shock during Acquisition or drug treatment. **(B)** Half-session freezing in non-shock mice. (Supp. Table 1, rows 80). **(C)** Number of longitudinally registered neurons in non-shock mice. **(D)** Sum of session discriminability index. Because roughly half the number of neurons were recorded in non-shock mice as in the other two groups, pooled tensors from psilocybin responders, non-responders, and saline mice were subsampled to a different, random set of 160 neurons in each of 100 iterations of TCA. One-Way ANOVA. (Supp. Table 1, rows 81). **(E)** Overlap of the *Day 2*-dominant ensemble with *Day 3*- and *Day 5*-dominant ensembles in non-shock mice. Bar graphs display the median fraction overlaps. Dots are individual animals. Insets are pie charts displaying total overlap. Stars indicate comparison to saline distribution. Chi-square. (Supp. Table 1, rows 82). **(F)** Same as E) for the *Day 3*-dominant ensemble. Chi-square. (Supp. Table 1, rows 83). **(G)** Same as F) for the *Day 5*-dominant ensemble. Chi-square. (Supp. Table 1, rows 84). **(H)** Average z-score with respect to *Day 2* of *Day 2*-dominant ensemble during *Day 3* and *5* in non-shock mice (black) compared to conditioned, saline-administered mice. Two-Way RM ANOVA. (Supp. Table 1, rows 85). **(I)** Same as H) for the *Day 3*-dominant ensemble. (Supp. Table 1, rows 86). **(J)** Same as F) for the *Day 5*-dominant ensemble. (Supp. Table 1, rows 87). Data are represented as mean ± SEM. * $p \leq 0.05$, ** $p < 0.01$, *** $p < 0.001$, **** $p < 0.0001$

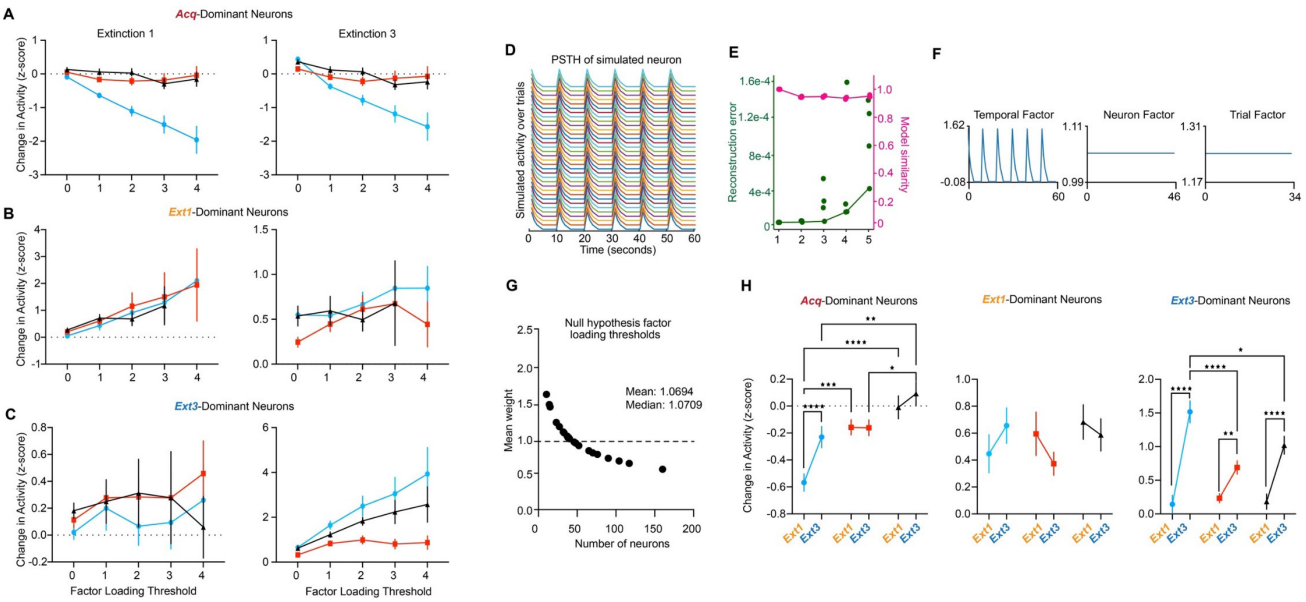

Supplementary Figure 6 | Results are robust to changes in factor loading thresholds.
(A) Change in activity in mean ± SEM from *Acquisition* in *Acq*-dominant neurons as a function of factor loading thresholds varying between *w*=0-4 during *Extinction 1* (left) and *Extinction 3* (right). **(B)** Same as A) for *Ext1*-dominant neurons. **(C)** Same as A) for *Ext3*-dominant neurons. **(D)** PSTH of an example simulated neuron to determine the null hypothesis factor loading threshold. Tensors of t x c x T size, where c is the number of neurons recorded in a given animal, were created with identically behaving neurons to determine the factor loading threshold in a hypothetical population in which each neuron equally contributes to dynamics, or the null hypothesis factor loading threshold for that animal. **(E)** Reconstruction error and model similarity of varying model ranks for populations of identical neurons. A model of rank 1 yields 0 error in this case. **(F)** Representative rank 1 TCA of a simulated dataset with n=46 neurons, the median number of neurons recorded in this study. Because variances across trials and neurons were clamped at 0, only the temporal factor varies. **(G)** Data in Fig. 4A plotted as a function of number of neurons recorded. Mean weight of neuron factors across 100 iterations of TCA at the number of cells recorded in each animal. **(H)** Change in activity in mean ± SEM from *Acquisition* during *Extinction 1* and *3* in *Acq*-dominant (left), *Ext1*-dominant (middle), and *Ext3*-dominant (right) using ensembles determined with the null hypothesis factor loading for each animal. Two-way RM ANOVA. (Supp. Table 1, rows 88-90) . * $p \leq 0.05$, ** $p < 0.01$, *** $p < 0.001$, **** $p < 0.0001$

Supplementary Table 1

Row	Figure	Statistical Model	Variable	Degrees of Freedom	Parameter(s)	Paramter value	p-value	Multiple comparisons? (Tukey or Sidak test)	p-value	n per group
			Treatment			1.324	0.2555			
			Time			3.733	0.0592			
1	Fig. 1B, panel 1	Two Way RM-ANOVA	Interaction	(1,49)	F-statistic	2.056	0.158			25 mice
			Treatment			1.485	0.2289			
			Time			535.4	<0.0001			
2	Fig. 1B, panel 2	Two Way RM-ANOVA	Interaction	(1,49)	F-statistic	1.435	0.2367			25 mice
			Treatment			0.7684	0.0349	Early, Late	Early: 0.0426; Late: 0.2236	
			Time			12.87	0.0008			
3	Fig. 1B, panel 3	Two Way RM-ANOVA	Interaction	(1,49)	F-statistic	4.75	0.385			25 mice
			Treatment			3.242	0.0779			
			Time			7.294	0.0095			
4	Fig. 1B, panel 4	Two Way RM-ANOVA	Interaction	(1,49)	F-statistic	6.545	0.0137	Early, Late	Early: 0.0254, Late: 0.6244	25 mice
			Treatment			2.592	0.1139			
			Time			2.577	0.1149			
5	Fig. 1B, panel 5	Two Way RM-ANOVA	Interaction	(1,49)	F-statistic	1.045	0.3117			25 mice
6	Fig. 1C	Unpaired t-test	Treatment	49	1.763		0.0841			25 mice
			Treatment	(3,46)		0.6896	0.5631			
			Time	(1,46)		2.507	0.1202			
7	Fig. 1D, panel 1	Two Way RM-ANOVA	Interaction	(3,46)	F-statistic	0.7442	0.5312			7-18 mice
			Treatment	(3,46)		0.4031	0.7514			
			Time	(1,46)		485.7	<0.0001			
8	Fig. 1D, panel 2	Two Way RM-ANOVA	Interaction	(3,46)	F-statistic	5.867	0.0018			7-18 mice
			Treatment	(3,46)		7.711	0.0003	Early, Late	Early: Sal RE vs. Psil RE 0.0503; Sal RE vs. Sal SE 0.2747; Sal RE vs. Psil SE 0.6575; Psil RE vs. Sal SE: 0.0016; Psil RE vs. Psil SE 0.0131; Sal SE vs. Psil SE 0.9468. Late: Sal RE vs. Psil RE 0.0424; Sal RE vs. Sal SE 0.9608; Sal RE vs. Psil SE 0.2775; Psil RE vs. Sal SE: 0.0669 Psil RE vs. Psil SE 0.0014; Sal SE vs. Psil SE 0.6935.	
			Time	(1,46)		11.49	0.0014		0.0014	
9	Fig. 1D, panel 3	Two Way RM-ANOVA	Interaction	(3,46)	F-statistic	1.031	0.3875		0.3875	7-18 mice
			Treatment	(3,46)		8.448	0.0001	Early, Late	Early: Sal RE vs. Psil RE 0.0051; Sal RE vs. Sal SE 0.6994; Sal RE vs. Psil SE 0.5599; Psil RE vs. Sal SE: 0.0025; Psil RE vs. Psil SE 0.0012; Sal SE vs. Psil SE 0.9977. Late: Sal RE vs. Psil RE 0.5469; Sal RE vs. Sal SE 0.0871; Sal RE vs. Psil SE 0.0190; Psil RE vs. Sal SE: 0.0058; Psil RE vs. Psil SE 0.0008; Sal SE vs. Psil SE 0.9598	
			Time	(1,46)		3.196	0.0804		0.0804	
10	Fig. 1D, panel 4	Two Way RM-ANOVA	Interaction	(3,46)	F-statistic	3.209	0.0316		0.0316	7-18 mice
			Treatment	(3,46)		40.12	0.0001	Early, Late	Early: Sal RE vs. Psil RE 0.6883; Sal RE vs. Sal SE <0.0001; Sal RE vs. Psil SE 0.0012; Psil RE vs. Sal SE <0.0001; Psil RE vs. Psil SE <0.0001; Sal SE vs. Psil SE 0.5327. Late: Sal RE vs. Psil RE 0.3257; Sal RE vs. Sal SE <0.0001; Sal RE vs. Psil SE 0.0001; Psil RE vs. Sal SE <0.0001; Psil RE vs. Psil SE <0.0001; Sal SE vs. Psil SE 0.0551.	
			Time	(1,46)		5.449	0.024	Early, Late		
11	Fig. 1D, panel 5	Two Way RM-ANOVA	Interaction	(3,46)	F-statistic	1.585	0.2058	Early, Late		7-18 mice
14	Fig. 1F, panel 1	Logistic regression	Extinction rate class		beta0/log likelihood/ auROC	1.599±1.256 / 0.3262 / 0.6032	0.5690 / 0.5679 / 0.4314			7-18 mice
			Group	(9, 207)		17.38	0.0004	Session half	Res vs. Non-Res: Hab:>0.9999, 0.9942 Acq: 0.3009, 0.7430 Ext1: 0.7947, 0.9997 Ext2: 0.9969, 0.4925 Ext3: 0.3079, 0.0012	
			Time	(2.406, 55.34)		33.75	<0.0001			
15	Fig. 1F, panel 2	Two Way RM-ANOVA	Interaction	(1,23)	F-statistic	17.38	<0.0001			7-18 mice
12	Fig. 1G, panel 1	Logistic regression	Extinction rate class		beta0/log likelihood/ auROC	2.896±1.065 / 7.0057 / 0.8333	0.0173 / 0.0057 / 0.0077			7-18 mice
			Group	(9, 207)		10.64	<0.0001	Session half	Res vs. Non-Res: Hab:0.9773, 0.9945, Acq: 0.9951, >0.9999, Ext1: 0.0943, 0.0399, Ext2: 0.3355, 0.0104, Ext3: 0.1489, <0.0001	
			Time	(2.406, 55.34)		47.5	<0.0001			
13	Fig. 1G, panel 2	Two Way RM-ANOVA	Interaction	(1,23)	F-statistic	27.86	<0.0001			7-18 mice

Row	Figure	Statistical Model	Variable	Degrees of Freedom	Parameter(s)	Paramter value	p-value	Multiple comparisons? (Tukey or Sidak test)	p-value	n per group
			Group	(2, 18)		2	0.1644			
			Time	(3.797, 68.34)		1.419	0.2388			
16	Fig. 2F, panel 1	Two Way RM-ANOVA	Interaction	(14, 126)	F-statistic	1	0.3893			7 mice
			Group	(2, 18)		0.9146	0.4185			
			Time	(3.797, 68.34)		25.81	<0.0001			
17	Fig. 2F, panel 2	Two Way RM-ANOVA	Interaction	(14, 126)	F-statistic	0.6924	0.7784			7 mice
			Group	(2, 18)		0.6316	0.5431			
			Time	(4.160, 74.88)		1.052	0.3878			
18	Fig. 2F, panel 3	Two Way RM-ANOVA	Interaction	(10, 90)	F-statistic	0.5085	0.8259			7 mice
			Group	(2, 18)		1.087	0.3585			
			Time	(4.160, 74.88)		1.424	0.2341			
19	Fig. 2F, panel 4	Two Way RM-ANOVA	Interaction	(10, 90)	F-statistic	0.4903	0.8923			7 mice
			Group	(2, 18)		0.5553	0.0041	Trials	Trial 1: Res vs. Non 0.2722; Res vs. Sal 0.604; Non vs. Sal 0.7936 Trial 2: Res vs. Non 0.0906; Res vs. Sal 0.0539; Non vs. Sal 0.9995 Trial 3: Res vs. Non 0.3456; Res vs. Sal 0.9233; Non vs. Sal 0.5482 Trial 4: Res vs. Non 0.0273; Res vs. Sal 0.0306; Non vs. Sal 0.5561 Trial 5: Res vs. Non 0.1547; Res vs. Sal 0.2504; Non vs. Sal 0.9328 Trial 6: Res vs. Non 0.1222; Res vs. Sal 0.3889; Non vs. Sal 0.8055	
			Time	(4.160, 74.88)		1.267	0.2934			
20	Fig. 2F, panel 5	Two Way RM-ANOVA	Interaction	(10, 90)	F-statistic	0.5533	0.8458			7 mice
21	Fig. 2F, panel 6	One Way RM-ANOVA	Group	(2, 18)	F-statistic	1.254	0.0215	Comparing psilocybin groups to saline	Res vs. Sal = 0.0499; Non vs. Sal = 0.8411	7 mice
			Group	(2,18)		0.5398	0.592			
			Time	(2.753, 49.55)		0.8443	0.4644			
22	Fig. 2J	Two Way RM ANOVA	Interaction	(8,72)	F-statistic	1.206	0.3077			7 mice
			Group	(2,18)		0.1042	0.9016			
			Time	(2.753, 49.55)		7.096	0.0003			
23	Fig. 2K	Two Way RM ANOVA	Interaction	(8,72)	F-statistic	1.048	0.4088			7 mice
			Group	(2,18)		0.0623	0.9398			
			Time	(2.753, 49.55)		2.775	0.0428			
24	Fig. 2L	Two Way RM ANOVA	Interaction	(8,72)	F-statistic	0.4335	0.897			7 mice
			Group	(2,18)		1.437	0.2637			
			Time	(2.753, 49.55)		29.21	<0.0001			
25	Fig. 2M	Two Way RM ANOVA	Interaction	(8,72)	F-statistic	0.3027	0.9627			7 mice
			Group	(2,18)		0.4478	0.6459			
			Time	(2.753, 49.55)		13.75	<0.0001			
26	Fig. 2P	Two Way RM ANOVA	Interaction	(8,72)	F-statistic	1.63	0.1313			7 mice
			Sex	(2,18)		0.6052	0.5581			
			Time	(5.778, 104.2)		16.53	<0.0001			
27	Fig. 3B, panel 1	Two Way RM ANOVA	Interaction	(66, 594)	F-statistic	0.8329	0.8223			7 mice
			Sex	(2,18)		1.285	0.3229			
			Time	(5.778, 104.2)		13.74	<0.0001			
28	Fig. 3B, panel 2	Two Way RM ANOVA	Interaction	(66, 594)	F-statistic	1.204	0.0103			7 mice
			Sex	(2,18)		0.2697	0.7667			
			Time	(5.778, 104.2)		9.13	<0.0001			
29	Fig. 3B, panel 3	Two Way RM ANOVA	Interaction	(66, 594)	F-statistic	0.8547	0.7847			7 mice
			Sex	(2,18)		4.231	0.3596			
			Time	(5.778, 104.2)		20.28	<0.0001			
30	Fig. 3B, panel 4	Two Way RM ANOVA	Interaction	(66, 594)	F-statistic	1.058	0.0312			7 mice
			Sex	(2,18)		0.2277	0.7987			
			Time	(5.778, 104.2)		16.43	<0.0001			
31	Fig. 3B, panel 5	Two Way RM ANOVA	Interaction	(66, 594)	F-statistic	1.042	0.3911			7 mice
32	Fig. 3C, solid	Ordinary One-Way ANOVA	Group	(2, 18)	F-statistic	0.5407	0.5915			7 mice
33	Fig. 3C, checkered	Ordinary One-Way ANOVA	Group	(2, 18)	F-statistic	0.4984	0.6156			7 mice
34	Fig. 3D	Multiple unpaired t-tests	Dateset (real vs. shuffled)	198	t-statistic	144.1; 115.9; 155.9	<0.0001; <0.0001; <0.0001			100 iterations
35	Fig. 3E - data for	Multiple linear regression	Component trial factor weight X trial by trial freezing		F-statistic/R2	for each animal (res, nonres, sal): 24.2871 0.8126 7.262 0.5646 10.0595 0.6424 2.7637 0.3304 5.1204 0.4776 6.6871 0.5442 4.7136 0.457 8.9874 0.6161 5.2324 0.483 3.8343 0.4064 5.7258 0.5056 1.7432 0.2374 8.4946 0.6027 4.3268 0.4359 3.3388 0.3735 3.2644 0.3683 5.7293 0.5057 4.2004 0.4286 3.1072 0.3569 2.0108 0.2642 2.4635 0.3055	for each animal (res, nonres, sal): 0 0 0.0002 0.0016 0 0.009 0.0376 0.0009 0.0019 0.1575 0.0003 0.0001 0.003 0.0048 0.0172 0.0191 0.0009 0.0057 0.0235 0.1079 0.0571			21 mice

Row	Figure	Statistical Model	Variable	Degrees of Freedom	Parameter(s)	Paramter value	p-value	Multiple comparisons? (Tukey or Sidak test)	p-value	n per group
36	Fig. 3E	Wilcoxon rank-sum	Median correlation between component trial factor weight X trial by trial freezing > 0		Sum of signed ranks	res: 28.0/ non-res: 28.0/ sal: 28.0	res: 0.0156; non-res: 0.0156; sal: 0.0156			
37	Fig. 3F, column 1	Linear regression	Strength of component in session X extinction rate	(1,19)	F-statistic/Beta0/ R2	H: 0.6973 / -0.07817 / 0.03540; A: 0.4962, / 0.05690 / 0.02545; E1 0.6020 / 0.05855 / 0.03071; E2: 0.1427/ 0.01963 / 0.007452; E3: 0.4347 / 0.04096 / 0.02237	H: 0.4141, A: 0.4897, E1: 0.4474, E2: 0.7098, E3 0.5176			21 mice
38	Fig. 3F, column 2	Linear regression	Strength of component in session X extinction rate	(1,19)	F-statistic/Beta0/ R2	H: 0.2515/ 0.04533 / 0.01306; A: 2.692 / -0.1296 / 0.1241; E1 -0.02112 / -0.02112 / 0.002113; E2: 0.1427/ 0.0755 / 0.05979; E3: 0.4347 / 0.09385 / 0.1285	H: 0.6218, A: 0.1173, E1: 0.8431, E2: 0.2854, E3 0.1106			21 mice
39	Fig. 3F, column 3	Linear regression	Strength of component in session X extinction rate	(1,19)	F-statistic/Beta0/ R2	H: 0.1744 / -0.03684 / 0.009095; A: 0.4962, / -0.02452 / 0.005961; E1 2.394 / -0.1309 / 0.1119; E2: 0.2255/ -0.0564 / 0.01173; E3: 0.04184 /-0.02214 / 0.002197	H: 0.6809, A: 0.7394, E1: 0.1383, E2: 0.6403, E3 0.8401			21 mice
40	Fig. 3F, column 4	Linear regression	Strength of component in session X extinction rate	(1,19)	F-statistic/Beta0/ R2	H: 2.029 / 0.1275 / 0.0965; A: 0.03238, / -0.01209 0.001701; E1 0.006821 / -0.008477 / 0.0003589; E2: 5.533/ -0.1994 / 0.2255; E3: 0.2794 / 0.03526 / 0.01449	H: 0.1705, A: 0.8591, E1: 0.935, E2: 0.0296, E3 0.6032			21 mice
41	Fig. 3F, column 5	Linear regression	Strength of component in session X extinction rate	(1,19)	F-statistic/Beta0/ R2	H: 0.06392 / 0.02579 / 0.003353; A: 2.43, / 0.07323 / 0.1134; E1 0.218 / 0.05245 / 0.01134; E2: 0.9223/ 0.0414 / 0.0463; E3: 10.8 /-0.2158 / 0.3624	H: 0.8031, A: 0.1355, E1: 0.6459, E2: 0.3489, E3 0.0039			21 mice
42	Fig. 3G	Linear regression	Component strength X extinction rate	(1,19)	F-statistic/Beta0/ R2	11.74 / -1.579±0. 4607 / 0.3820	0.0028			21 mice
43	Fig. 4B, top	Chi-square	Group	3	Chi-square	Res vs. Sal: 31.17; Res v Nonres: 6.433; Nonres v sal: 21.64	Res vs. Sal <0. 0001, Res v nonres: 0.0923; Nonres v sal: <0.0001			7 mice
44	Fig. 4B, middle	Chi-square	Group	3	Chi-square	Res vs. Sal: 33.31; Res v Nonres: 2.092; Nonres v sal: 32.49	Res vs. Sal <0. 0001, Res v nonres: 0.5536; Nonres v sal: <0.0001			7 mice
45	Fig. 4B, bottom	Chi-square	Group	3	Chi-square	Res vs. Sal: 34.77; Res v Nonres: . 2397; Nonres v sal: 33.49	Res vs. Sal <0. 0001, Res v nonres: 0.9709; Nonres v sal: <0.0001			7 mice
46	Fig. 4D, top	Wilcoxon rank-sum	Median = 0		sum of signed ranks	R1: -1849, R3: -1794, N1 -1415, N3 -1173, S1 -151, S3 -123	R1 <0.0001, R3 <0.0001, N1 <0. 0001, N3 <0. 0001, S1 < 0.0001, S3 0.0021			63 neurons (R), 53 neurons (N), 17 neurons (S)
47	Fig. 4D, bottom	Two Way RM ANOVA	Group	(2, 130)	F-statistic	4.734	0.0104	Ext1, Ext3	Ext1: Res vs. Non 0.0143; Res vs. Sal 0.9972; Non vs. Sal 0.1667 Ext3: Res vs. Non 0.0183; Res vs. Sal 0.9972; Non vs. Sal 0.1667	63 neurons (R), 53 neurons (N), 17 neurons (S)
			Time	(1, 130)		2.965	0.0875			
			Interaction	(2, 130)		0.01344	0.9866			
48	Fig. 4E, top	Wilcoxon rank-sum	Median = 0		sum of signed ranks	R1: 493, R3: 489, N1 754, N3 326, S1 183, S3 5	R1 0.0010, R3 0.0011, N1 <0. 0001, N3 0.0856, S1 0.0007, S3 0.9383			41 neurons (R), 47 neurons (N), 21 neurons (S)
49	Fig. 4E, bottom	Two Way RM ANOVA	Group	(2, 106)	F-statistic	1.845	0.163	Res, Non-Res, Sal	Res: Ext1 vs. Ext3 0.0488; Non: Ext1 vs. Ext3 0.2563; Sal: Ext1 vs. Ext3 0.0020	41 neurons (R), 47 neurons (N), 21 neurons (S)
			Time	(1, 106)		20.77	0.0104			
			Interaction	(2, 106)		1.961	0.9866			
50	Fig. 4F, top	Wilcoxon rank-sum	Median = 0		sum of signed ranks	R1: 28, R3: 1784, N1 355, N3 941, S1 -30, S3 1766	R1 0.9214, R3 <0.0001, N1 0.0525, N3 <0. 0001, S1 0.9215, S3 < 0.0001			60 neurons (R), 46 neurons (N), 63 neurons (S)
51	Fig. 4F, bottom	Two Way RM ANOVA	Group	(2, 166)	F-statistic	3.808	0.0004	Ext1, Ext3	Ext1: Res vs. Non 0.9941; Res vs. Sal 0.9992; Non vs. Sal 0.9814 Ext3: Res vs. Non <0.0001; Res vs. Sal 0.0058; Non vs. Sal 0.1667	60 neurons (R), 46 neurons (N), 63 neurons (S)
			Time	(1, 166)		93.35	<0.0001	Res, Non-Res, Sal	Res: Ext1 vs. Ext3 <0.0001; Non: Ext1 vs. Ext3 0.0281 Sal: Ext1 vs. Ext3 0.0020	
			Interaction	(2, 166)		8.095	0.0004			

Row	Figure	Statistical Model	Variable	Degrees of Freedom	Parameter(s)	Paramter value	p-value	Multiple comparisons? (Tukey or Sidak test)	p-value	n per group
52	Fig. 4G, top	WIlcoxon rank-sum	Median = 0		sum of signed ranks	R1: -307, R3: -465, N1 -48, N3 -328, S1 209, S3 -249	R1 0.0077, R3 <0.0001, N1 0.5979, N3 <0.0001, S1 0.4235, S3 < 0.0001			34 neurons (R), 28 neurons (N), 58 neurons (S)
53	Fig. 4G, bottom	Two Way RM ANOVA	Group	(2, 117)	F-statistic	6.869	0.0015	Ext1, Ext3	Ext1: Res vs. Non 0.9941; Res vs. Sal 0.9992; Non vs. Sal 0.9814 Ext3: Res vs. Non <0.0001; Res vs. Sal 0.0058; Non vs. Sal 0.1667	34 neurons (R), 28 neurons (N), 58 neurons (S
			Time	(1, 117)		22.41	<0.0001	Res, Non-Res, Sal	Res: Ext1 vs. Ext3 <0.0001; Non: Ext1 vs. Ext3 0.0281 Sal: Ext1 vs. Ext3 0.0020	
			Interaction	(2, 117)		0.6691	0.5141		0.5141	
54	Fig. 4H, top	WIlcoxon rank-sum	Median = 0		sum of signed ranks	R1: -210, R3: 16, N1 -187, N3 -19, S1 -119, S3 31	R1 <0.0001, R3 0.0049, N1 0.0005, N3 0.7593, S1 0.4235, S3 0.4874			20 neurons (R), 21 neurons (N), 17 neurons (S)
55	Fig. 4H, bottom	Two Way RM ANOVA	Group	(2, 55)	F-statistic	8.81	0.0005	Ext1, Ext3	Ext1: Res vs. Non 0.3823; Res vs. Sal 0.9866; Non vs. Sal 0.6256 Ext3: Res vs. Non 0.0057; Res vs. Sal 0.2539; Non vs. Sal 0.4583	20 neurons (R), 21 neurons (N), 17 neurons (S)
			Time	(1, 55)		75.07	<0.0001	Res, Non-Res, Sal	Res: Ext1 vs. Ext3 <0.0001; Non: Ext1 vs. Ext3 0.1052 Sal: Ext1 vs. Ext3 <0.0001	
			Interaction	(2, 55)		0.6069	0.5472			
56	Fig. 4I, top	WIlcoxon rank-sum	Median = 0		sum of signed ranks	R1: 693, R3: 1035, N1 368, N3 490, S1 93, S3 93	R1 <0.0001, R3 <0.0001, N1 0.0003, N3 <0.0001, S1 0.4016, S3 0.0016			45 neurons (R), 32 neurons (N), 14 neurons (S)
57	Fig. 4I, bottom	Two Way RM ANOVA	Group	(2, 55)	F-statistic	3.698	0.0287	Ext1, Ext3	Ext1: Res vs. Non 0.6246; Res vs. Sal 0.0562; Non vs. Sal 0.0124 Ext3: Res vs. Non 0.4873; Res vs. Sal 0.7068; Non vs. Sal 0.2545	45 neurons (R), 32 neurons (N), 14 neurons (S)
			Time	(1, 55)		0.9934	0.3216	Res, Non-Res, Sal		
			Interaction	(2, 55)		0.9202	0.4022			
58	Fig. 4J, top	WIlcoxon rank-sum	Median = 0		sum of signed ranks	R1: -165, R3: 69, N1 265, N3 263, S1 561, S3 1023	R1 0.0255, R3 0.3666, N1 0.0032, N3 0.0035, S1 0.0437, S3 0.0002			25 neurons (R), 29 neurons (N), 61 neurons (S))
59	Fig. 4J, bottom	Two Way RM ANOVA	Group	(2, 112)	F-statistic	5.609	0.0048	Ext1, Ext3	Ext1: Res vs. Non 0.6246; Res vs. Sal 0.0562; Non vs. Sal 0.0124 Ext3: Res vs. Non 0.4873; Res vs. Sal 0.7068; Non vs. Sal 0.2545	25 neurons (R), 29 neurons (N), 61 neurons (S)
			Time	(1, 112)		16.18	0.0001	Res, Non-Res, Sal	Res: Ext1 vs. Ext3 0.0083; Non: Ext1 vs. Ext3 0.2714 Sal: Ext1 vs. Ext3 0.0704	
			Interaction	(2, 112)		0.9663	0.3836			
60	Fig. 5B, top	WIlcoxon rank-sum	Median = 0		sum of signed ranks	R1: -8126, R3: -4531, N1 -3852, N3 -2972, S1 -845, S3 144	R1<0.0001, R3 <0.0001, N1 <0.0001, N3 0.0006, S1 0.4339, S3 0.8946			142 neurons (R), 131 neurons (N), 151 neurons (S)
61	Fig. 5B, bottom	Two Way RM ANOVA	Group	(2, 421)	F-statistic	2.582	<0.0001	Ext1, Ext3	Ext1: Res vs. Non 0.0001; Res vs. Sal <0.0001; Non vs. Sal 0.0926 Ext3: Res vs. Non 0.0512; Res vs. Sal <0.0001; Non vs. Sal 0.1396	142 neurons (R), 131 neurons (N), 151 neurons (S)
			Time	(1, 421)		8.488	0.0038	Res, Non-Res, Sal	Res: Ext1 vs. Ext3 0.0014; Non: Ext1 vs. Ext3 0.7703; Sal: Ext1 vs. Ext3 0.8857	
			Interaction	(2, 421)		2.582	0.0768			
62	Fig. 5C, top	WIlcoxon rank-sum	Median = 0		sum of signed ranks	R1: 2229, R3: 4645, N1 4941, N3 2719, S1 2852, S3 3105	R1 0.0276, R3 <0.0001, N1 <0.0001, N3 0.0001, S1 0.0122, S3 0.0063			145 neurons (R), 137 neurons (N), 157 neurons (S)
63	Fig. 5C, bottom	Two Way RM ANOVA	Group	(2, 436)	F-statistic	0.9478	0.3884			145 neurons (R), 137 neurons (N), 157 neurons (S)
			Time	(1, 436)		0.1251	0.7237			
			Interaction	(2, 436)		0.7409	0.4773			
64	Fig. 5D, top	WIlcoxon rank-sum	Median = 0		sum of signed ranks	R1: 157, R3: 9921, N1 2606, N3 5870, S1 -4708, S3 9761	R1 0.8840, R3 <0.0001, N1 0.0018, N3 <0.0001, S1 0.0004, S3 <0.0001			145 neurons (R), 137 neurons (N), 175 neurons (S)
65	Fig. 5D, bottom	Two Way RM ANOVA	Group	(2, 450)	F-statistic	8.085	0.0004	Ext1, Ext3	Ext1: Res vs. Non 0.9690; Res vs. Sal 0.1153 ; Non vs. Sal 0.0508 Ext3: Res vs. Non <0.0001; Res vs. Sal <0.0001; Non vs. Sal 0.9968	145 neurons (R), 128 neurons (N), 175 neurons (S)
			Time	(1, 450)		136.5	0.0001	Res, Non-Res, Sal	Res: Ext1 vs. Ext3 <0.0001; Non: Ext1 vs. Ext3 0.0035; Sal: Ext1 vs. Ext3 <0.0001	
			Interaction	(2, 450)		8.3	0.0003			
66	Supp Fig. 1A panel 1	Two Way RM ANOVA	Treatment	(1,49)	F-statistic	2.242	0.1407			25 mice
			Time	(3.046,149.2)		0.7415	0.5308			
			Interaction	(7, 343)		1.216	0.2932			

Row	Figure	Statistical Model	Variable	Degrees of Freedom	Parameter(s)	Paramter value	p-value	Multiple comparisons? (Tukey or Sidak test)	p-value	n per group
			Treatment	(1,49)		3.492	0.0678			
			Time	(3.046,149.2)		157.3	<0.0001			
67	Supp Fig. 1A panel 2	Two Way RM ANOVA	Interaction	(7, 343)	F-statistic	0.5099	0.8272			25 mice
			Treatment	(1,49)		6.308	0.0154	Trials	Sal vs. Psil: Trial 1 0.1652; 0.2923; 0.0041; 0.1476; 0.8648; 0.9992	
			Time	(4.573,224.1)		9.31	<0.0001			
68	Supp Fig. 1A panel 3	Two Way RM ANOVA	Interaction	(5, 245)	F-statistic	3.818	0.0024			25 mice
			Treatment	(1,49)		2.693	0.1072			
			Time	(4.573,224.1)		1.653	0.1641			
69	Supp Fig. 1A panel 4	Two Way RM ANOVA	Interaction	(5, 245)	F-statistic	2.084	0.068			25 mice
			Treatment	(1,49)		1.318	0.2565			
			Time	(3.046,149.2)		3.6585	0.0092			
70	Supp Fig. 1A panel 5	Two Way RM ANOVA	Interaction	(7, 343)	F-statistic	0.5474	0.7402			25 mice
			Sex	(1,23)		0.7097	0.6593			
			Time	(3.770,86.72)		26.52	<0.0001			
71	Supp Fig. 1B	Two Way RM ANOVA	Interaction	(23, 207)	F-statistic	1.161	0.953			7-18 mice
			Sex	(1,23)		0.003543	0.2172			
			Time	(1.790,41.8)		34.28	<0.0001			
72	Supp Fig. 1C	Two Way RM ANOVA	Interaction	(9, 207)	F-statistic	0.7537	0.6997			7-18 mice
			Treatment	(1,23)		1.037	0.2172			
			Time	(2.629, 68.36)		15.83	<0.0001			
73	Supp Fig. 1D	Two Way RM ANOVA	Interaction	(9, 234)	F-statistic	4.074	<0.0001			9-17 mice
			Treatment	(2,18)		1.183	0.3291			
			Time	(3.351,60.32)		10.41	<0.0001			
74	Supp Fig. 2B	Two Way RM ANOVA	Interaction	(8,72)	F-statistic	0.8232	0.5849			
			Sex	(2,18)		1.099	0.3546			
			Time	(5.972, 107.5)		1.103	0.3654			
75	Supp Fig. 3A	Two Way RM ANOVA	Interaction	(118, 1062)	F-statistic	0.9765	0.554			7 mice
			Sex	(2,18)		0.4514	0.6438			
			Time	(5.972, 107.5)		4.479	0.0014			
76	Supp Fig. 3B	Two Way RM ANOVA	Interaction	(118, 1062)	F-statistic	1.234	0.0533			7 mice
			Sex	(2,18)		1.73	0.2055			
			Time	(5.972, 107.5)		0.9667	0.4509			
77	Supp Fig. 3C	Two Way RM ANOVA	Interaction	(118, 1062)	F-statistic	0.9184	0.7178			7 mice
			Sex	(2,18)		2.71	0.0936			
			Time	(5.972, 107.5)		1.544	0.1821			
78	Supp Fig. 3D	Two Way RM ANOVA	Interaction	(118, 1062)	F-statistic	0.4021	0.9999			7 mice
			Sex	(2,18)		0.3126	0.7354			
			Time	(5.972, 107.5)		1.243	0.2975			
79	Supp Fig. 3E	Two Way RM ANOVA	Interaction	(118, 1062)	F-statistic	1.205	0.0769			7 mice
80	Supp Fig. 5B	One Way RM ANOVA	Time	(9,20)	F-statistic	0.6529	0.5091			3 mice
81	Supp. Fig. 5D	One Way ANOVA	Group	(3, 396)	F-statistic	55.71	<0.0001	Compare to non-shock	All comparisons: <0.0001	100 iterations
82	Supp. Fig. 5E	Chi-square	Group (Non-shock v. Saline)	3	Chi-square	23.85	<0.0001			
83	Supp. Fig. 5F	Chi-square	Group (Non-shock v. Saline)	3	Chi-square	37.73	<0.0001			
84	Supp. Fig. 5G	Chi-square	Group (Non-shock v. Saline)	3	Chi-square	56.13	<0.0001			
			Group	(1, 227)		10.76	0.0012	Sal vs. Nonshock	Ext1: 0.0149, Ext3: 0.0061	
			Time	(1, 227)		0.1684	0.6819			
85	Supp Fig. 5H	Two Way RM ANOVA	Interaction	(1, 227)	F-statistic	0.08495	0.771			151 saline, 78 non-shock neurons
			Group	(1, 224)		2.25	0.238			
			Time	(1, 224)		1.135	0.2879			
86	Supp Fig. 5I	Two Way RM ANOVA	Interaction	(1, 224)	F-statistic	2.25	0.135			158 saline, 69 non-shock neurons
			Group	(1, 256)		1.551	0.1948			
			Time	(1, 256)		76.18	<0.0001			
87	Supp Fig. 5J	Two Way RM ANOVA	Interaction	(1, 256)	F-statistic	6.403	0.0201	Sal vs. Nonshock	Ext1: 0.9611, Ext3: 0.0337	175 saline, 83 non-shock neurons
			Group	(2, 479)		12.11	<0.0001	Ext1, Ext3	Ext1: Res vs. Non 0.0003; Res vs. Sal < 0.0001 Non vs. Sal 0.3995 Ext3: Res vs. Non 0.8865; Res vs. Sal 0.0034; Non vs. Sal 0.0322	
			Time	(1, 479)		14.01	0.0002	Res, Non-Res, Sal	Res: < 0.0001; Non: >0.9999 ; Sal: 0.2474	
88	Supp. Fig. 6H, left	Two Way RM ANOVA	Interaction	(2, 479)	F-statistic	6	0.0022			142 neurons (R), 131 neurons (N), 167 neurons (S)
			Group	(2, 481)		0.3818	0.6829			
			Time	(1, 481)		0.2102	0.6468			
89	Supp. Fig. 6H, middle	Two Way RM ANOVA	Interaction	(2, 481)	F-statistic	2.424	0.0896			178 neurons (R), 148 neurons (N), 158 neurons (S)

Row	Figure	Statistical Model	Variable	Degrees of Freedom	Parameter(s)	Paramter value	p-value	Multiple comparisons? (Tukey or Sidak test)	p-value	n per group
			Group	(2, 484)		2.864	<0.0001	Ext1, Ext3	Ext1: Res vs. Non 0.9469; Res vs. Sal 0.9972 Non vs. Sal 0.9840 Ext3: Res vs. Non <0.0001; Res vs. Sal 0.0374; Non vs. Sal 0.1111	
			Time	(1, 484)		122.8	<0.0001	Res, Non-Res, Sal	Res: < 0.0001; Non: 0.0076 ; Sal:< 0.0001	171 neurons (R), 144 neurons (N), 171 neurons (S)
90	Fig. 5D, right	Two Way RM ANOVA	Interaction	(2, 484)	F-statistic	10.13	0.058			